SANDIA REPORT
SAND2020-9992
Printed September 2020

Sandia National Laboratories

Bistatic Synthetic Aperture Radar – Issues, Analysis, and Design

Armin W Doerry

Prepared by
Sandia National Laboratories
Albuquerque, New Mexico
87185 and Livermore,
California 94550

Issued by Sandia National Laboratories, operated for the United States Department of Energy by National Technology & Engineering Solutions of Sandia, LLC.

Available to DOE and DOE contractors from
U.S. Department of Energy
Office of Scientific and Technical Information
P.O. Box 62
Oak Ridge, TN 37831

Telephone: (865) 576-8401
Facsimile: (865) 576-5728
E-Mail: reports@osti.gov
Online ordering: http://www.osti.gov/scitech

Available to the public from
U.S. Department of Commerce
National Technical Information Service
5301 Shawnee Rd
Alexandria, VA 22312

Telephone: (800) 553-6847
Facsimile: (703) 605-6900
E-Mail: orders@ntis.gov
Online order: https://classic.ntis.gov/help/order-methods/

Abstract

The physical separation of the transmitter from the receiver into perhaps separate flight vehicles (with separate flight paths) in a bistatic Synthetic Aperture radar system adds considerable complexity to an already complex system. Synchronization of waveform parameters and timing attributes become problematic, and notions of even the synthetic aperture itself take on a new level of abstractness. Consequently, a high-performance, fine-resolution, and reliable bistatic SAR system really needs to be engineered from the ground up, with tighter specifications on a number of parameters, and entirely new functionality in other areas. Nevertheless, such a bistatic SAR system appears viable.

Acknowledgements

This report was funded by General Atomics Aeronautical Systems, Inc. (GA-ASI) Mission Systems under Cooperative Research and Development Agreement (CRADA) SC08/01749 between Sandia National Laboratories and GA-ASI.

General Atomics Aeronautical Systems, Inc. (GA-ASI), an affiliate of privately-held General Atomics, is a leading manufacturer of Remotely Piloted Aircraft (RPA) systems, radars, and electro-optic and related mission systems, including the Predator®/Gray Eagle®-series and Lynx® Multi-mode Radar.

As with most of the author's professional accomplishments, we are grateful for the advice and counsel of many talented and insightful colleagues. These include Doug Bickel, Tim Bielek, Dale Dubbert, Ted Kim, all of Sandia National Laboratories.

Contents

List of Figures

"Before I refuse to take your questions, I have an opening statement."
-- Ronald Reagan

Acronyms and Definitions

1-D, 2-D, 3-D	1-, 2-, 3-Dimesional
ADC	Analog to Digital Converter
APC	Antenna Phase Center
CPI	Coherent Processing Interval
DDS	Direct Digital Synthesis/Synthesizer
GPS	Global Positioning System
IF	Intermediate Frequency
GMTI	Ground Moving Target Indicator [radar]
LO	Local Oscillator
LFM	Linear Frequency Modulated
MCP	Motion Compensation Point
MDV	Minimum Detectable Velocity
MIMO	Multiple-Input Multiple-Output
NBSS	Notional Bistatic SAR System
PGA	Phase Gradient Autofocus
PRI	Pulse Repetition Interval
PRF	Pulse Repetition Frequency
RX	Receiver
SAR	Synthetic Aperture Radar
SRP	Scene Reference Point
SNR	Signal to Noise Ratio
STALO	STAble Local Oscillator
T&C	Timing and Control
TX	Transmitter

Foreword

This report details the results of an academic study. It does not presently exemplify any modes, methodologies, or techniques employed by any operational system known to the author.

This report shares some development with, and updates and expands discussion with respect to, an earlier limited-distribution report from 2000. The references to specific testbed systems that were the impetus for limiting the distribution of the earlier report have all been removed. What remains is a purely academic treatment of the topic, with at most some generic non-descript comments regarding anecdotal support.

Classification

The specific mathematics and algorithms presented herein do not bear any release restrictions or distribution limitations.

This report formalizes preexisting informal notes and other documentation on the subject matter herein.

Author Contact Information

Armin Doerry awdoerr@sandia.gov 505-845-8165

1 Introduction

Bistatic radar refers to the condition where the antenna transmitting the radar illumination energy and the antenna receiving the target echo energy are not collocated. Specifically, we identify an antenna's location, and in fact the radar's location, as the location of its Antenna Phase Center (APC). In the strict sense, any antenna under motion exhibits this characteristic since echoes exhibit a finite non-zero delay time. Usually, however, bistatic conjures a notion of separate and distinct transmitting and receiving antennas, that may or may not ride the same vehicle.

Making sense of the bistatic radar echoes can be quite challenging, especially if relative motion exists between the two antennas and perhaps the target. This is the expected case for imaging with bistatic Synthetic Aperture Radar (SAR). The bistatic geometry significantly complicates the imaging problem over the monostatic case. A typical scenario is where the transmitter is located on one airborne (or spaceborne) vehicle, and the receiver is located on another airborne (or spaceborne) vehicle. Another less obvious scenario is where the two antennae are located on different parts of an aircraft exhibiting angular rotations, such as with a long-baseline Interferometric SAR implementation.

An excellent text detailing many aspects of bistatic radar generally is by Willis and Griffiths.[1]

The published literature has a number of papers that examine the relationship of range and Doppler measurements in various bistatic geometries, and generally allude to the difficulties of processing bistatic data into usable images. Additionally, a number of bistatic experiments and data collections have been conducted over the years, to examine various aspects of bistatic imaging and system engineering, often with impressive results.[2,3,4]

With many prior experiments, often out of economic necessity, the underlying presumptions are to collect the data with relatively simple (usually kluged up monostatic SAR) systems, and then do complicated processing to make usable images. A more long-term rational approach might be to study the underlying bistatic problem and engineer a truly bistatic imaging solution that collects data in an optimal fashion to simplify the image formation processing, thereby making the highest quality images achievable. We like this latter approach better.

Consequently, this report deals with issues and analysis for engineering a bistatic SAR system.

"People who think they know everything are a great annoyance to those of us who do."
-- Isaac Asimov

2 Basic Bistatic Concepts

The bistatic SAR system geometry is defined by the location of three entities:

1) the Transmitter (TX) antenna,

2) the Receiver (RX) antenna, and

3) the target scene.

We make the usual presumption that the target is static and ambivalent to the imaging process. The actual image is formed by the receiver, so we make the additional presumption that the receiver always knows its own geometric relationship to the target scene. The big unknown is usually what the receiver knows about the transmitter, both its geometric relationship to the other entities, and its signal properties. Consequently, we can talk about several classes of bistatic SAR systems.

Class 1: Fully Cooperative TX

In this case, the RX is fully aware of the TX geometry and signal properties, and furthermore the TX is aware enough of the RX to actively assist in modifying its geometry and/or signal properties to facilitate image formation by the RX. The TX and RX work together as a team, each actively helping the other.

Class 2: Friendly but Ambivalent TX

In this case the TX is unaware of the RX geometry and does not actively help it by modifying its signal properties beyond pointing its beam in the proper direction to illuminate the target scene. The RX is aware, however, of the TX geometry and signal properties to an extent sufficient to considerably improve the data collection and image formation process. The TX is quite likely engineered to be predictable in some manner, and/or has some sort of enhanced observability to the RX image formation process.

Class 3: Unfriendly and Ambivalent TX

In this case the TX is completely unaware of the RX, and furthermore, knowledge of the TX geometry and signal properties is unavailable to the RX except by observation of the TX signal itself. The TX is quite likely a transmitter of opportunity that was not specifically engineered for bistatic SAR operation. The TX just happens to be there, otherwise the RX is on its own.

Class 4: Unfriendly and Hostile TX

In this case the TX actively attempts to prevent use by an undesired remote receiver in a bistatic fashion. It perhaps deliberately makes its waveform unusable to an undesired RX by perhaps employing random phase coding, or equivalent. The RX needs to find utility in a TX signal deliberately meant to obfuscate image formation.

Of these, the Class 4 bistatic SAR systems are the hardest to make work reliably. We will ignore this specific problem in this report.

If a single transmitter is used with multiple receivers, then the system is termed multistatic, rather than merely bistatic. In such a system the TX must service multiple RX geometries simultaneously. This diminishes the attractiveness of Class 1 operation, which causes the single TX to be slaved to a single RX. Consequently, to facilitate eventual multistatic operation, we will not consider Class 1 operation further.

Class 2 and Class 3 operation differ only in the availability of ancillary TX geometry and signal property information to the RX. Clearly, the more that the RX knows about the TX, the easier the image formation task becomes. The remainder of this report addresses these two classes of operation.

We also comment that a relatively recent popular area of research interest has been the Multiple-Input Multiple-Output (MIMO) system architecture. As its name implies, multiple transmitters emit signals whose echoes are captured by multiple receivers, with no guarantee that any of the transmitters and/or receivers are collocated.[5] While MIMO systems must also contend with basic bistatic system performance issues, specifically addressing unique challenges to MIMO radar is beyond the scope of this report.

3 Bistatic Phase-History Data

What follows is a development of the phase-history data model; a model of the raw radar echoes as ultimately down-converted and ready for processing into a range-Doppler image. We will presume the waveform is the popular Linear Frequency Modulated (LFM) chirp signal, and that "stretch" processing is employed, whereby the receiver mixes the echo with a Local Oscillator (LO) chirp to partially range-compress the echo by removing the chirp characteristic, also known as "deramping."[6]

The intent here is to develop an accurate data model, useful and in fact necessary for image formation. Specific image formation algorithms themselves are beyond the scope of this report.

3.1 Phase-History Simplified Model

Following the phase history model development in earlier reports, we present here the development of a model for the bistatic phase-history collected by the receiver. But first we define the geometry as displayed in Figure 1.

In this geometry we define

MCP = Motion Compensation Point, a reference point in the SAR image,
s = vector from MCP to a specific target point,
$\mathbf{r}_{c1}$ = vector from MCP to the transmitter,
$\mathbf{r}_{c2}$ = vector from MCP to the receiver,
$\mathbf{r}_{s1}$ = vector from the target point to the transmitter, and
$\mathbf{r}_{s2}$ = vector from the same target point to the receiver. (1)

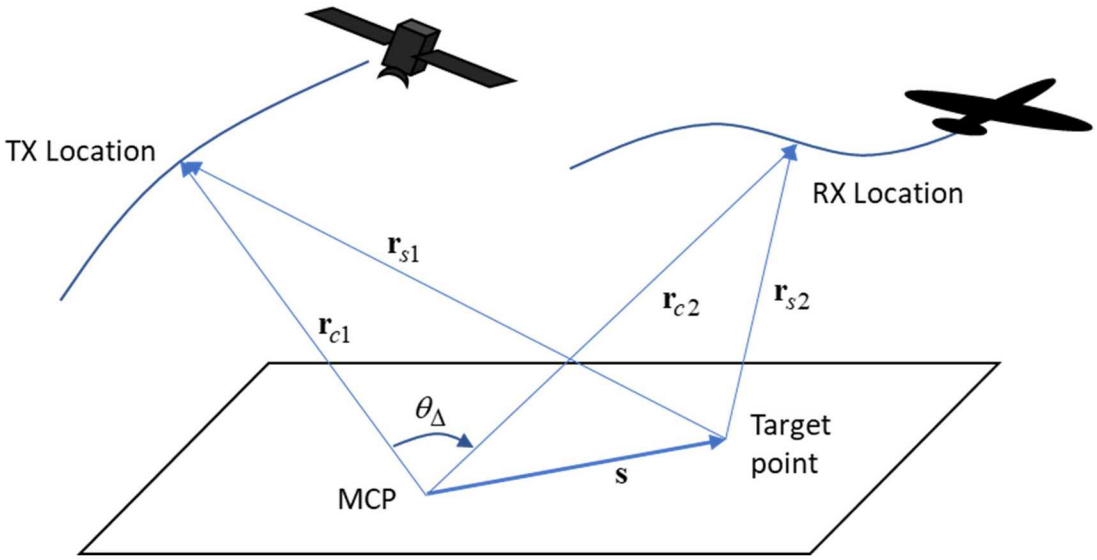

Figure 1. Bistatic SAR geometry.

The MCP is also sometimes called the Scene Reference Point (SRP) and may go by other names as well.

Transmitted Phase

The instantaneous phase of the transmitted signal is presumed to be quadratic (yielding an LFM chirp), and is given by

$$\Phi_{TX} = \phi_T + \omega_T \left(t - t_0 - t_n\right) + \frac{\gamma_T}{2}\left(t - t_0 - t_n\right)^2, \tag{2}$$

where

ϕ_T = reference phase of the TX signal,
ω_T = reference center frequency of the TX signal,
γ_T = reference chirp rate of the TX signal,
t_n = reference time for a particular TX pulse, and
t_0 = offset time to center of the TX pulse. (3)

We will ignore the pulse envelope for this development. We state only that the envelopes are suitably known and accounted for in the phase history data collection.

Received Phase

The phase of the received echo is a suitably time-delayed version of the transmitted phase, given by

$$\Phi_{RX} = \phi_T + \omega_T \left(t - t_0 - t_n - t_s\right) + \frac{\gamma_T}{2}\left(t - t_0 - t_n - t_s\right)^2, \tag{4}$$

where the echo delay time of the target is given by

$$t_s = \frac{1}{c}\left(\left|\mathbf{r}_{s1}\right| + \left|\mathbf{r}_{s2}\right|\right). \tag{5}$$

Let us further define a reference delay time as the echo delay time of the MCP itself, or

$$t_c = \frac{1}{c}\left(\left|\mathbf{r}_{c1}\right| + \left|\mathbf{r}_{c2}\right|\right). \tag{6}$$

For the moment, we assume this to be a known constant for any one pulse. That is, no intra-pulse Doppler effects. Furthermore, this implies that the TX motion is completely known, as well as its timing, which is wrapped up in $\left(t - t_0 - t_n\right)$.

Then the RX phase can be manipulated to

$$\Phi_{RX} = \phi_T + \omega_T\left(t - t_0 - t_n - t_c + t_c - t_s\right) + \frac{\gamma_T}{2}\left(t - t_0 - t_n - t_c + t_c - t_s\right)^2$$

$$= \left\{ \begin{aligned} &\phi_T + \omega_T\left(t - t_0 - t_n - t_c\right) + \frac{\gamma_T}{2}\left(t - t_0 - t_n - t_c\right)^2 \\ &+\omega_T\left(t_c - t_s\right) + \gamma_T\left(t - t_0 - t_n - t_c\right)\left(t_c - t_s\right) + \frac{\gamma_T}{2}\left(t_c - t_s\right)^2 \end{aligned} \right\}$$

$$= \left\{ \begin{aligned} &\phi_T + \omega_T\left(t - t_0 - t_n - t_c\right) + \frac{\gamma_T}{2}\left(t - t_0 - t_n - t_c\right)^2 \\ &+\left[\omega_T + \gamma_T\left(t - t_0 - t_n - t_c\right)\right]\left(t_c - t_s\right) + \frac{\gamma_T}{2}\left(t_c - t_s\right)^2 \end{aligned} \right\}. \tag{7}$$

Note that time delay difference can be manipulated to

$$\begin{aligned} \left(t_c - t_s\right) &= \frac{1}{c}\left(\left|\mathbf{r}_{c1}\right| + \left|\mathbf{r}_{c2}\right|\right) - \frac{1}{c}\left(\left|\mathbf{r}_{s1}\right| + \left|\mathbf{r}_{s2}\right|\right) \\ &= \frac{1}{c}\left(\left|\mathbf{r}_{c1}\right| - \left|\mathbf{r}_{s1}\right|\right) + \frac{1}{c}\left(\left|\mathbf{r}_{c2}\right| - \left|\mathbf{r}_{s2}\right|\right). \end{aligned} \tag{8}$$

The Local Oscillator

The purpose of the Local Oscillator (LO) in the receiver is to remove the chirp, down-convert, and to stabilize the phase history if possible. For stretch processing, the LO waveform is also an LFM chirp with phase is given by

$$\Phi_{LO} = \phi_L + \omega_L\left(t - t_0 - t_{n'} - t_m\right) + \frac{\gamma_L}{2}\left(t - t_0 - t_{n'} - t_m\right)^2, \tag{9}$$

where

t_m = offset delay of LO pulse center from TX pulse center, and
$t_{n'}$ = presumed (or estimated) reference time of the TX pulse by the receiver. (10)

We strongly desire that that the receiver's LO accurately estimates $t_{n'} = t_n$, but we expect this to be perhaps difficult to achieve in practice. Consequently, we will allow them to differ, unless otherwise stated.

The Video Phase

The video phase is the difference between the RX phase and the LO phase. This is manipulated as follows,

$$
\begin{aligned}
\Phi_V &= \Phi_{RX} - \Phi_{LO} \\
&= \left\{ \begin{array}{l} \phi_T + \omega_T \left(t - t_0 - t_n - t_c\right) + \frac{\gamma_T}{2}\left(t - t_0 - t_n - t_c\right)^2 \\ + \left[\omega_T + \gamma_T \left(t - t_0 - t_n - t_c\right)\right]\left(t_c - t_s\right) + \frac{\gamma_T}{2}\left(t_c - t_s\right)^2 \\ - \phi_L - \omega_L \left(t - t_0 - t_{n'} - t_m\right) - \frac{\gamma_L}{2}\left(t - t_0 - t_{n'} - t_m\right)^2 \end{array} \right\} \\
&= \left\{ \begin{array}{l} \left[\omega_T + \gamma_T \left(t - t_0 - t_n - t_c\right)\right]\left(t_c - t_s\right) + \frac{\gamma_T}{2}\left(t_c - t_s\right)^2 \\ + \phi_T - \phi_L + \omega_T \left(t - t_0 - t_n - t_c\right) - \omega_L \left(t - t_0 - t_{n'} - t_m\right) \\ + \frac{\gamma_T}{2}\left(t - t_0 - t_n - t_c\right)^2 - \frac{\gamma_L}{2}\left(t - t_0 - t_{n'} - t_m\right)^2 \end{array} \right\} \\
&= \left\{ \begin{array}{l} \left[\omega_T + \gamma_T \left(t - t_0 - t_n - t_c\right)\right]\left(t_c - t_s\right) + \frac{\gamma_T}{2}\left(t_c - t_s\right)^2 \\ + \phi_T - \phi_L + \omega_T \left(t - t_0 - t_{n'} - t_m + t_m - t_c + t_{n'} - t_n\right) - \omega_L \left(t - t_0 - t_{n'} - t_m\right) \\ + \frac{\gamma_T}{2}\left(t - t_0 - t_{n'} - t_m + t_m - t_c + t_{n'} - t_n\right)^2 - \frac{\gamma_L}{2}\left(t - t_0 - t_{n'} - t_m\right)^2 \end{array} \right\} \\
&= \left\{ \begin{array}{l} \left[\omega_T + \gamma_T \left(t - t_0 - t_n - t_c\right)\right]\left(t_c - t_s\right) + \frac{\gamma_T}{2}\left(t_c - t_s\right)^2 \\ + \phi_T - \phi_L + \omega_T \left(t_m - t_c + t_{n'} - t_n\right) + \omega_T \left(t - t_0 - t_{n'} - t_m\right) - \omega_L \left(t - t_0 - t_{n'} - t_m\right) \\ + \frac{\gamma_T}{2}\left(t_m - t_c + t_{n'} - t_n\right)^2 + \gamma_T \left(t_m - t_c + t_{n'} - t_n\right)\left(t - t_0 - t_{n'} - t_m\right) \\ + \frac{\gamma_T}{2}\left(t - t_0 - t_{n'} - t_m\right)^2 - \frac{\gamma_L}{2}\left(t - t_0 - t_{n'} - t_m\right)^2 \end{array} \right\}
\end{aligned} \tag{11}
$$

and finally,

$$
\Phi_V = \left\{ \begin{array}{l} \left[\omega_T + \gamma_T \left(t - t_0 - t_n - t_c\right)\right]\left(t_c - t_s\right) + \frac{\gamma_T}{2}\left(t_c - t_s\right)^2 \\ + \left[\phi_T - \phi_L + \omega_T \left(t_m - t_c + t_{n'} - t_n\right) + \frac{\gamma_T}{2}\left(t_m - t_c + t_{n'} - t_n\right)^2\right] \\ + \left[\omega_T + \gamma_T \left(t_m - t_c + t_{n'} - t_n\right) - \omega_L\right]\left(t - t_0 - t_{n'} - t_m\right) \\ + \left[\frac{\gamma_T}{2} - \frac{\gamma_L}{2}\right]\left(t - t_0 - t_{n'} - t_m\right)^2 \end{array} \right\}. \tag{12}
$$

It becomes useful to identify some specific time differences with shorthand parameters as

$\tau_{mc} = (t_m - t_c)$ = time difference between LO pulse center and MCP echo delay,
$\tau_{n'n} = (t_{n'} - t_n)$ = error in RX-estimated and true reference time of the TX pulse, and
$\tau_{sc} = -(t_c - t_s)$ = echo delay time offset of target point from MCP. (13)

Using these, the video phase then can be expressed as

$$\Phi_V = \left\{ \begin{array}{l} -\left[\omega_T + \gamma_T (t - t_0 - t_n - t_c)\right]\tau_{sc} + \frac{\gamma_T}{2}{\tau_{sc}}^2 \\ +\left[\phi_T - \phi_L + \omega_T(\tau_{mc} + \tau_{n'n}) + \frac{\gamma_T}{2}(\tau_{mc} + \tau_{n'n})^2\right] \\ +\left[\omega_T + \gamma_T(\tau_{mc} + \tau_{n'n}) - \omega_L\right](t - t_0 - t_{n'} - t_m) \\ +\left[\frac{\gamma_T}{2} - \frac{\gamma_L}{2}\right](t - t_0 - t_{n'} - t_m)^2 \end{array} \right\}. \quad (14)$$

In this formulation, the target location influences the first line of the phase expression, and the LO waveform parameters influence the next three lines of the phase expression.

Motion Compensation with the LO

If we know the TX waveform parameters and all relevant timing information, then we can set the LO waveform parameters to cancel undesired phase terms, by setting

$$\begin{aligned} \phi_L &= \phi_T + \omega_T(\tau_{mc} + \tau_{n'n}) + \frac{\gamma_T}{2}(\tau_{mc} + \tau_{n'n})^2, \\ \omega_L &= \omega_T + \gamma_T(\tau_{mc} + \tau_{n'n}), \text{ and} \\ \gamma_L &= \gamma_T . \end{aligned} \quad (15)$$

If we can manage this, then this allows the video signal to be modeled as the considerably simplified expression

$$\Phi_V = \left\{ -\left[\omega_T + \gamma_T (t - t_0 - t_n - t_c)\right]\tau_{sc} + \frac{\gamma_T}{2}{\tau_{sc}}^2 \right\}. \quad (16)$$

This is essentially the common model for monostatic phase-history data. This would be very desirable, and points to the value of the receiver knowing TX timing and waveform parameters as accurately as possible.

For example, if we know the TX waveform parameters (chirp rate, frequency, and phase), but we don't know the TX waveform timing, and hence we don't know $\tau_{n'n}$, then this leads to some unresolvable phase errors, and the best we can do is to force LO waveform parameters to

$$\phi_L = \phi_T + \omega_T \tau_{mc} + \frac{\gamma_T}{2} {\tau_{mc}}^2 ,$$
$$\omega_L = \omega_T + \gamma_T \tau_{mc} , \text{ and}$$
$$\gamma_L = \gamma_T . \tag{17}$$

This leaves us with the video phase containing additional undesired terms (i.e. error terms), and described by the more complicated expression

$$\Phi_V = \left\{ \begin{array}{l} -\left[\omega_T + \gamma_T \left(t - t_0 - t_n - t_c \right) \right] \tau_{sc} + \frac{\gamma_T}{2} {\tau_{sc}}^2 \\ + \left[\left(\omega_T + \gamma_T \tau_{mc} \right) \tau_{n'n} + \frac{\gamma_T}{2} {\tau_{n'n}}^2 \right] \\ + \left[\gamma_T \tau_{n'n} \right] \left(t - t_0 - t_{n'} - t_m \right) \end{array} \right\} . \tag{18}$$

This shows that an inaccurate estimate for $t_{n'}$ will cause a phase error and frequency offset, neither of which, if held constant, is a big problem. If, however, $t_{n'}$ changed during an aperture, such that there were a linear (or higher-order component) to $\tau_{n'n}$, then bad things start to happen, such as migration and misfocusing in the SAR image. This could very easily become quite severe.

Recall, however, that to achieve even this model, we need to know the TX waveform parameters ϕ_T, ω_T, and γ_T, and ultimately the TX flight path. Clearly, it is very desirable to know reference times t_n as well.

Extracting Target Coordinates

Now turn our attention to the unknown quantity τ_{sc}. Recall

$$\tau_{sc} = \left(t_s - t_c \right) = \frac{1}{c} \left(\left| \mathbf{r}_{s1} \right| - \left| \mathbf{r}_{c1} \right| \right) + \frac{1}{c} \left(\left| \mathbf{r}_{s2} \right| - \left| \mathbf{r}_{c2} \right| \right) . \tag{19}$$

If we define the target location vector (from the MCP) as **s**, then for the TX we have

$$\begin{aligned} \left| \mathbf{r}_{s1} \right| - \left| \mathbf{r}_{c1} \right| &= \left| \mathbf{r}_{c1} - \mathbf{s} \right| - \left| \mathbf{r}_{c1} \right| \\ &= \frac{-\mathbf{r}_{c1} \bullet \mathbf{s}}{\left| \mathbf{r}_{c1} \right|} + \xi_{n1} \\ &= -\mathbf{n}_{c1} \bullet \mathbf{s} + \xi_{n1} \end{aligned} \tag{20}$$

where

$\mathbf{n}_{c1}$ = the unit vector pointing towards the TX from the MCP, and

$$\xi_{n1} = \left(|\mathbf{r}_{s1}| - |\mathbf{r}_{c1}|\right) + \left(\mathbf{n}_{c1} \bullet \mathbf{s}\right) \text{ = undesired error terms.} \tag{21}$$

Similarly, for the RX we define

$$\begin{aligned} |\mathbf{r}_{s2}| - |\mathbf{r}_{c2}| &= |\mathbf{r}_{c2} - \mathbf{s}| - |\mathbf{r}_{c2}| \\ &= \frac{-\mathbf{r}_{c2} \bullet \mathbf{s}}{|\mathbf{r}_{c2}|} + \xi_{n2} \\ &= -\mathbf{n}_{c2} \bullet \mathbf{s} + \xi_{n2} \end{aligned} \tag{22}$$

where

$\mathbf{n}_{c2}$ = the unit vector pointing towards the RX from the MCP, and

$$\xi_{n2} = \left(|\mathbf{r}_{s2}| - |\mathbf{r}_{c2}|\right) + \left(\mathbf{n}_{c2} \bullet \mathbf{s}\right) \text{ = undesired error terms.} \tag{23}$$

Consequently, we may expand

$$\begin{aligned} \tau_{sc} &= \frac{1}{c}\left(|\mathbf{r}_{s1}| - |\mathbf{r}_{c1}|\right) + \frac{1}{c}\left(|\mathbf{r}_{s2}| - |\mathbf{r}_{c2}|\right) \\ &= \frac{1}{c}\left(-\mathbf{n}_{c1} \bullet \mathbf{s} + \xi_{n1}\right) + \frac{1}{c}\left(-\mathbf{n}_{c2} \bullet \mathbf{s} + \xi_{n2}\right) \\ &= \frac{1}{c}\left[-\left(\mathbf{n}_{c1} + \mathbf{n}_{c2}\right) \bullet \mathbf{s} + \left(\xi_{n1} + \xi_{n2}\right)\right]. \end{aligned} \tag{24}$$

Note that the vectors $\mathbf{n}_{c1}$ and $\mathbf{n}_{c2}$ are both unit vectors, but their sum is not. Let us define a new unit vector as in the direction of their sum, that is

$$\mathbf{n}_c = \frac{\mathbf{n}_{c1} + \mathbf{n}_{c2}}{|\mathbf{n}_{c1} + \mathbf{n}_{c2}|}. \tag{25}$$

Analyzing this with respect to Figure 1 reveals that

$$|\mathbf{n}_{c1} + \mathbf{n}_{c2}| = 2\cos\left(\frac{\theta_\Delta}{2}\right). \tag{26}$$

where

θ_Δ = the angular difference between vectors $\mathbf{n}_{c1}$ and $\mathbf{n}_{c2}$. (27)

Note that the orientation of this angle depends strictly on the vectors $\mathbf{n}_{c1}$ and $\mathbf{n}_{c2}$, and is not in any other particular geometric plane. Furthermore, $\mathbf{n}_c$ bisects the angle between vectors $\mathbf{n}_{c1}$ and $\mathbf{n}_{c2}$, but only in the unique plane defined by vectors $\mathbf{n}_{c1}$ and $\mathbf{n}_{c2}$. For an arbitrary plane, the

projection of $\mathbf{n}_c$ onto that plane does not necessarily bisect the projections of vectors $\mathbf{n}_{c1}$ and $\mathbf{n}_{c2}$ onto that same plane. More on this later.

Consequently, we can expand the target's relative delay to

$$\tau_{sc} = \frac{1}{c}\left[-2\cos\left(\frac{\theta_\Delta}{2}\right)\left(\mathbf{n}_c \bullet \mathbf{s}\right) + 2\xi_n \right]. \tag{28}$$

where the error terms have been averaged to

$$\xi_n = \frac{\xi_{n1} + \xi_{n2}}{2}. \tag{29}$$

This single error term encompasses all the spatially-variant phase error phenomena across the aperture(s), such as wavefront curvature, etc.

We can rewrite τ_{sc} as

$$\tau_{sc} = \frac{2}{c}\cos\left(\frac{\theta_\Delta}{2}\right)\left[-\left(\mathbf{n}_c \bullet \mathbf{s}\right) + \xi_n \Big/ \cos\left(\frac{\theta_\Delta}{2}\right)\right]. \tag{30}$$

Putting this all together into the video phase, and assuming for the moment that $\tau_{n'n} = 0$, yields

$$\Phi_V = \left\{ \begin{array}{l} \dfrac{2}{c}\left[\omega_T + \gamma_T\left(t - t_0 - t_n - t_c\right)\right]\cos\left(\dfrac{\theta_\Delta}{2}\right)\left[\left(\mathbf{n}_c \bullet \mathbf{s}\right) - \xi_n \Big/ \cos\left(\dfrac{\theta_\Delta}{2}\right)\right] \\ + \dfrac{2\gamma_T}{c^2}\cos^2\left(\dfrac{\theta_\Delta}{2}\right)\left[-\left(\mathbf{n}_c \bullet \mathbf{s}\right) + \xi_n \Big/ \cos\left(\dfrac{\theta_\Delta}{2}\right)\right]^2 \end{array} \right\}. \tag{31}$$

Also, for the moment, let us ignore error terms, as well as the residual video phase error term (the 2nd line in the equation). This leaves the desired quantity

$$\Phi_V = \left\{ \frac{2}{c}\left[\omega_T + \gamma_T\left(t - t_0 - t_n - t_c\right)\right]\cos\left(\frac{\theta_\Delta}{2}\right)\left(\mathbf{n}_c \bullet \mathbf{s}\right) \right\}. \tag{32}$$

Note that this differs from the monostatic case only by the new definition of $\mathbf{n}_c$ and the scaling of all frequencies (and equivalently bandwidths and wavenumbers) by $\cos\left(\theta_\Delta/2\right)$.

An important point here is that to accurately assess the impact of target location **s** onto Φ_V, and to ultimately accurately extract **s** from Φ_V, we need to know with some accuracy the quantities θ_Δ and $\mathbf{n}_c$. Of course, this means we need to know with some degree of accuracy both the RX and the TX flight paths.

3.2 More on TX and RX Flight Paths

The TX flight path is defined to be the collection of all positions $\mathbf{r}_{c1} = |\mathbf{r}_{c1}|\mathbf{n}_{c1}$ over any particular aperture. This can be expressed as a polar coordinate frame 3-tuple $\left(|\mathbf{r}_{c1}|, \theta_{c1}, \psi_{c1}\right)$ where

$$\begin{aligned} &\theta_{c1} = \text{an azimuth angle (in the ground plane) from the MCP to the TX, and} \\ &\psi_{c1} = \text{an elevation angle from the MCP to the TX.} \end{aligned} \tag{33}$$

The SAR image focal plane is usually taken to be $\psi_{c1} = 0$.

Clearly, $\mathbf{n}_{c1}$ is uniquely defined by just these two angles as

$$\mathbf{n}_{c1} = \hat{\mathbf{x}}\cos\psi_{c1}\sin\theta_{c1} - \hat{\mathbf{y}}\cos\psi_{c1}\cos\theta_{c1} + \hat{\mathbf{z}}\sin\psi_{c1}. \tag{34}$$

Similarly, the RX flight path is defined to be the collection of all positions $\mathbf{r}_{c2} = |\mathbf{r}_{c2}|\mathbf{n}_{c2}$ over any particular aperture. This can be expressed as a polar coordinate frame 3-tuple in the same frame as the TX vector as $\left(|\mathbf{r}_{c2}|, \theta_{c2}, \psi_{c2}\right)$ where

$$\begin{aligned} &\theta_{c2} = \text{an azimuth angle (in the ground plane) from the MCP to the RX, and} \\ &\psi_{c2} = \text{an elevation angle from the MCP to the RX.} \end{aligned} \tag{35}$$

The plane $\psi_{c2} = 0$ is the same SAR image focal plane $\psi_{c1} = 0$.

Clearly, $\mathbf{n}_{c2}$ is uniquely defined by just these two angles as

$$\mathbf{n}_{c2} = \hat{\mathbf{x}}\cos\psi_{c2}\sin\theta_{c2} - \hat{\mathbf{y}}\cos\psi_{c2}\cos\theta_{c2} + \hat{\mathbf{z}}\sin\psi_{c2}. \tag{36}$$

Consequently, the sum of the unit vectors

$$\left(\mathbf{n}_{c1} + \mathbf{n}_{c2}\right) = \begin{Bmatrix} \hat{\mathbf{x}}\left(\cos\psi_{c1}\sin\theta_{c1} + \cos\psi_{c2}\sin\theta_{c2}\right) \\ -\hat{\mathbf{y}}\left(\cos\psi_{c1}\cos\theta_{c1} + \cos\psi_{c2}\cos\theta_{c2}\right) \\ +\hat{\mathbf{z}}\left(\sin\psi_{c1} + \sin\psi_{c2}\right) \end{Bmatrix}, \tag{37}$$

making the bisecting unit vector

$$\mathbf{n}_c = \begin{Bmatrix} \hat{\mathbf{x}}\left(\cos\psi_{c1}\sin\theta_{c1} + \cos\psi_{c2}\sin\theta_{c2}\right) \\ -\hat{\mathbf{y}}\left(\cos\psi_{c1}\cos\theta_{c1} + \cos\psi_{c2}\cos\theta_{c2}\right) \\ +\hat{\mathbf{z}}\left(\sin\psi_{c1} + \sin\psi_{c2}\right) \end{Bmatrix} \Bigg/ 2\cos\left(\frac{\theta_\Delta}{2}\right). \tag{38}$$

Effective Phase Center

Recall that the desired model for the video phase is given by

$$\Phi_V = \left\{ \frac{2}{c} \left[\omega_T + \gamma_T \left(t - t_0 - t_n - t_c \right) \right] \cos\left(\frac{\theta_\Delta}{2} \right) \left(\mathbf{n}_c \bullet \mathbf{s} \right) \right\}. \tag{39}$$

The parameters of this that are directly due to the geometry are $\mathbf{n}_c$, θ_Δ, and t_c. Recall also that $t_c = \left(|\mathbf{r}_{c1}| + |\mathbf{r}_{c2}| \right) / c$. If we define an equivalent monostatic range to scene center as the mean of the TX and RX ranges, that is

$$|\mathbf{r}_c| = \left(|\mathbf{r}_{c1}| + |\mathbf{r}_{c2}| \right) / 2, \tag{40}$$

then we can write the scene center delay as the more familiar expression

$$t_c = 2|\mathbf{r}_c| / c. \tag{41}$$

With these definitions we can identify an equivalent or effective phase center as the vector

$$\mathbf{r}_c = |\mathbf{r}_c| \mathbf{n}_c = \frac{\left(|\mathbf{r}_{c1}| + |\mathbf{r}_{c2}| \right)}{2} \mathbf{n}_c. \tag{42}$$

What this means is that a flat scene of isotropic resolution cells imaged with a bistatic SAR (with TX at $\mathbf{r}_{c1}$ and RX at $\mathbf{r}_{c2}$) will appear the same as if it might have been imaged with a monostatic SAR with collocated TX and RX at $\mathbf{r}_c$, and with frequencies scaled by $\cos\left(\theta_\Delta / 2 \right)$. These geometries are illustrated in Figure 2.

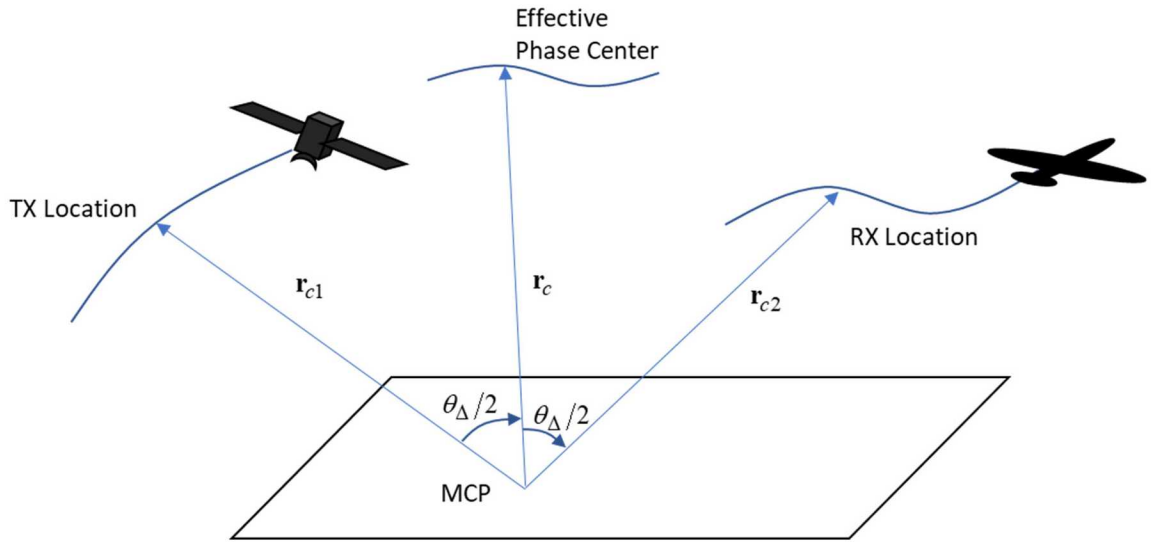

Figure 2. Bistatic SAR geometry.

The motion measurement problem can be reduced to tracking the effective phase center $\mathbf{r}_c$, and the bistatic angle θ_Δ. Doing so makes the bistatic imaging problem very similar to the monostatic imaging problem (in fact identical except for frequency scaling by a function of the bistatic angle θ_Δ). In any case, it is the motion of the effective phase center $\mathbf{r}_c$ that defines the effective synthetic aperture for collecting phase history data.

This is true of any cartesian frame. For convenience, let us presume that the image focal plane is the xy-plane. If we orient the x-axis and y-axis in the traditional respective cross-range and down-range directions in the ultimate image, then we can make the following points.

- For Doppler (or whatever the word 'Doppler' is meant to describe) to correspond to cross-range, we need a substantial variation in the term $\left(\cos\psi_{c1}\sin\theta_{c1}+\cos\psi_{c2}\sin\theta_{c2}\right)$. This can be had with a variation in either θ_{c1}, θ_{c2}, or both. But there is a caveat.
- It is possible to have TX and RX motion such that both θ_{c1} and θ_{c2} are varying substantially, but in such a way that the term $\left(\cos\psi_{c1}\sin\theta_{c1}+\cos\psi_{c2}\sin\theta_{c2}\right)$ is zero (e.g. the RX flying the same circle at the same angular rate but opposite direction than the TX). Doppler in this case will degenerate to anything but describing x-axis offset.
- The largest Doppler term will be had if θ_{c1} and θ_{c2} are both changing in the same angular direction. This leads to the shortest aperture collection time.
- The synthetic direction unit vector $\mathbf{n}_c$ bisects the angle between $\mathbf{n}_{c1}$ and $\mathbf{n}_{c2}$, but only in the unique plane defined by vectors $\mathbf{n}_{c1}$ and $\mathbf{n}_{c2}$. For an arbitrary plane, the projection of $\mathbf{n}_c$ onto that plane does not generally bisect the projections of vectors $\mathbf{n}_{c1}$ and $\mathbf{n}_{c2}$ onto that same plane. Consequently, for $\mathbf{n}_c$ described by

  $$\mathbf{n}_c=\hat{\mathbf{x}}\cos\psi_c\sin\theta_c-\hat{\mathbf{y}}\cos\psi_c\cos\theta_c+\hat{\mathbf{z}}\sin\psi_c\,, \tag{43}$$

  we are not assured that θ_c is the mean of θ_{c1} and θ_{c2}, and we are not assured that ψ_c is the mean of ψ_{c1} and ψ_{c2}.

  The projection of $\mathbf{n}_c$ bisects the angle between the projections of $\mathbf{n}_{c1}$ and $\mathbf{n}_{c2}$ only in planes where the projections of $\mathbf{n}_{c1}$ and $\mathbf{n}_{c2}$ are equal in length (e.g. in flight geometries where $\psi_{c1}=\psi_{c2}$).

  This is a particularly important point since several published papers and reports fail to correctly identify this, and in fact may identify it wrong.

Errors in knowing the TX flight path are basically motion measurement errors, in that the position of the effective phase center vs. time is not correctly known. Consequently, one might expect the same sort of image quality degradation as with monostatic SAR. One might also expect that autofocus could help considerably here, too, as long as we know the flight path 'good enough' for the residual errors to be within the capabilities of autofocus.

3.3 Sampling the Phase Histories

Digital samples are taken within a pulse echo at times

$$t = t_{n'} + t_0 + t_{ADC} + i\,T_s = t_n + t_0 + \tau_{n'n} + t_{ADC} + i\,T_s\,, \tag{44}$$

where the fast-time sample index is constrained to

$$-I/2 \le i < I/2\,. \tag{45}$$

Note that to properly place the fast-time samples, we need to know the pulse reference time t_n. Our best possible guess will be $t_{n'}$, which if precisely true would yield $\tau_{n'n} = 0$.

The things that can change from pulse to pulse are presumed to be just about everything except target vector ***s***, and propagation velocity *c*. Consequently, adding an aperture position index *n* to the appropriate parameters yields an expression for the video data as

$$\Phi_V = \left\{ \frac{2}{c}\left[\omega_{T,n} + \gamma_{T,n}\left(\tau_{n'n} + t_{ADC,n} + i\,T_{s,n} - t_{c,n} \right) \right] \cos\left(\frac{\theta_{\Delta,n}}{2} \right) \left(\mathbf{n}_{c,n} \bullet \mathbf{s} \right) \right\}, \tag{46}$$

where the aperture pulse position index is constrained to

$$-N/2 \le n < N/2\,. \tag{47}$$

Now we turn to the makings of $\left(\mathbf{n}_{c,n} \bullet \mathbf{s} \right)$. From earlier work, we can decompose this into polar coordinates to

$$\mathbf{n}_{c,n} \bullet \mathbf{s} = s_x \cos\psi_n \sin\alpha_n - s_y \cos\psi_n \cos\alpha_n + s_z \sin\psi_n\,, \tag{48}$$

where these angles are defined to be

$$\begin{aligned} \alpha_n &= \text{ground-plane azimuth angle from the MCP to the effective phase center, and} \\ \psi_n &= \text{an elevation angle from the MCP to the effective phase center.} \end{aligned} \tag{49}$$

We stipulate that the angle is confined to the span

$$-\alpha_{\max} \le \alpha_n \le \alpha_{\max}\,. \tag{50}$$

If we make the usual assumptions that $s_z = 0$, then a more convenient form becomes

$$\mathbf{n}_{c,n} \bullet \mathbf{s} = \cos\psi_n \cos\alpha_n \left(s_x \tan\alpha_n - s_y \right). \tag{51}$$

The video phase in Eq. (46) can now be written as

$$\Phi_V = \left\{ \begin{array}{c} \frac{2}{c}\left[\omega_{T,n} + \gamma_{T,n}\left(t_{ADC,n} + \tau_{n'n} - t_{c,n} + i\,T_{s,n} \right) \right] \cos\left(\frac{\theta_{\Delta,n}}{2} \right) \cos\psi_n \cos\alpha_n \\ \times \left(s_x \tan\alpha_n - s_y \right) \end{array} \right\}. \tag{52}$$

Now, for the moment, again assume that pulse timing is accurate and $\tau_{n'n} = 0$. This is highly desirable, and every attempt will be made to make this true.

The appropriate motion compensation operation becomes the adjusting of parameters such that

$$\begin{aligned} &\left[\omega_{T,n} + \gamma_{T,n}\left(t_{ADC,n} + \tau_{n'n} - t_{c,n} + i\,T_{s,n} \right) \right] \cos\left(\frac{\theta_{\Delta,n}}{2} \right) \cos\psi_n \cos\alpha_n \\ &\qquad = \left[\omega_0 + \gamma_0 T_{s0} i \right] \cos\left(\frac{\theta_{\Delta 0}}{2} \right) \cos\psi_{c0}\,. \end{aligned} \tag{53}$$

where the zero subscripts now denote nominal constants, at perhaps the center of the effective aperture. There are several ways that this might be achieved.

Note that if the TX is oblivious to the RX, we might set the TX waveform parameters to constant nominal values, say

$$\begin{aligned} &\omega_{T,n} = \omega_0, \text{ and} \\ &\gamma_{T,n} = \gamma_0\,. \end{aligned} \tag{54}$$

If these constant values were known to the RX, either a priori, or by being observable in some fashion, then we would optimally set at the RX the Analog to Digital Converter (ADC) sample spacing and timing offset as

$$\begin{aligned} &T_{s,n} = \kappa_n T_{s0}, \text{ and} \\ &t_{ADC,n} = t_{c,n} + \left(\kappa_n - 1 \right) \frac{\omega_0}{\gamma_0}, \end{aligned} \tag{55}$$

where the pulse-to-pulse scale factor is

$$\kappa_n = \frac{\cos\left(\frac{\theta_{\Delta 0}}{2} \right) \cos\psi_{c0}}{\cos\left(\frac{\theta_{\Delta,n}}{2} \right) \cos\psi_n \cos\alpha_n}. \tag{56}$$

Note how this scale factor now also depends on the bistatic angle $\theta_{\Delta,n}$. That is, proper motion compensation requires taking into account the instantaneous bistatic angle.[7,8,9]

The video phase of Eq. (52) now becomes (still assuming $\tau_{n'n} = 0$)

$$\Phi_V(i,n) = \left\{ \frac{2}{c}\left[\omega_0 + \gamma_0 T_{s0}\, i\right] \cos\left(\frac{\theta_{\Delta 0}}{2}\right) \cos\psi_{c0}\left(s_x \tan\alpha_n - s_y\right) \right\}. \tag{57}$$

The effective synthetic aperture depends on the variation in unit vector $\mathbf{n}_{c,n}$ which of course is a synthesized direction depending on both TX and RX unit vectors $\mathbf{n}_{c1}$ and $\mathbf{n}_{c2}$. Consequently, selecting optimal α_n to sample the spatial aperture requires knowledge of both TX and RX flight geometries. The more reasonable case is that the RX knows both flight geometries, but the TX knows only its own. However, spatial samples (and their angular positions α_n) are created by the TX. This presents a problem.

If the angles α_n are not precisely placed, then image quality suffers, mainly in a reduced focused scene size. If the α_n excessively wobble, then this may cause problematic azimuth sidelobes. Non-ideal spatial sample positions can be somewhat dealt with by appropriate phase-error corrections, but not entirely. Interpolating spatial samples to their proper position remains an option, but tends to be computationally expensive. The interpolation operation could be made easier by increasing the data oversampling factor (ultimately the Pulse Repetition Frequency, PRF) but at the expense of more data to collect.[10] An along-track autofocus operation could work, but still needs to be invented. In short, this area, while by no means a showstopper, could use a little work.

If, however, timing is not accurate and $\tau_{n'n} \neq 0$, and still ignoring residual video phase error and ξ_n, but including some of the LO terms thereby not cancelled, then with the other corrections identified we are left with the phase history model

$$\Phi_V(i,n) = \left\{ \begin{array}{l} \frac{2}{c}\left[\omega_0 + \gamma_0 T_{s0}\, i\right] \cos\left(\frac{\theta_{\Delta 0}}{2}\right) \cos\psi_{c0}\left(s_x \tan\alpha_n - s_y\right) \\ + \frac{2}{c}\left[\gamma_0\, \tau_{n'n}\right] \cos\left(\frac{\theta_{\Delta,n}}{2}\right) \cos\psi_n \cos\alpha_n \left(s_x \tan\alpha_n - s_y\right) \\ + \left(\omega_0 \kappa_n\right) \tau_{n'n} + \frac{\gamma_0}{2} {\tau_{n'n}}^2 + \left[\gamma_0 \kappa_n \tau_{n'n}\right] T_{s0}\, i \end{array} \right\}. \tag{58}$$

To first order we can approximate this with

$$\Phi_V(i,n) = \left\{ \begin{array}{l} \frac{2}{c}\left[\omega_0 + \gamma_0\, \tau_{n'n} + \gamma_0 T_{s0}\, i\right] \cos\left(\frac{\theta_{\Delta 0}}{2}\right) \cos\psi_{c0}\left(s_x \tan\alpha_n - s_y\right) \\ + \omega_0 \tau_{n'n} + \frac{\gamma_0}{2} {\tau_{n'n}}^2 + \left[\gamma_0 \tau_{n'n}\right] T_{s0}\, i \end{array} \right\}. \tag{59}$$

From this expression we see that non-zero $\tau_{n'n}$ will be perceived as errors in target position s_y (similar to a range error) and pulse-to-pulse variations in $\tau_{n'n}$ will affect the perception of target position s_x (similar to a line-of-sight velocity error).

3.4 Range and Azimuth Resolutions

From the phase history model, we can see that all frequencies and chirp-rates are scaled by $\cos(\theta_{\Delta 0}/2)$. This impacts resolution and pixel spacing in SAR images.

Range resolution is determined by the condition

$$\frac{2}{c}[\gamma_0 T_{s0} I]\cos\left(\frac{\theta_{\Delta 0}}{2}\right)\cos\psi_{c0}\left(\frac{\rho_y}{a_{wr}}\right) = 2\pi, \tag{60}$$

which can be transmogrified to explicitly calculating resolution as

$$\rho_y = \frac{a_{wr} c}{2B_{eff}\cos\psi_{c0}\cos\left(\frac{\theta_{\Delta 0}}{2}\right)}, \tag{61}$$

or, in the slant plane

$$\rho_r = \frac{a_{wr} c}{2B_{eff}\cos\left(\frac{\theta_{\Delta 0}}{2}\right)}, \tag{62}$$

where

ρ_y = ground-plane range resolution,
ρ_r = slant-plane range resolution,
a_{wr} = window broadening factor for range processing,[11]
$B_{eff} = \frac{\gamma_0 T_{s0} I}{2\pi}$ = effective chirp bandwidth in Hz. (63)

Azimuth resolution is determined by the condition

$$\frac{2}{c}\omega_0\cos\left(\frac{\theta_{\Delta 0}}{2}\right)\cos\psi_{c0}\left(\frac{\rho_x}{a_{wx}}\right)\left(2\tan\alpha_{\max}\right) = 2\pi, \tag{64}$$

which can be transmogrified to explicitly calculating resolution as

$$\rho_x = \frac{a_{wx}\lambda_0}{2\cos\left(\frac{\theta_{\Delta 0}}{2}\right)\cos\psi_{c0}\left(2\tan\alpha_{\max}\right)}, \tag{65}$$

where

ρ_x = azimuth resolution, and
a_{wx} = window broadening factor for cross-range (azimuth) processing,
$\lambda_0 = \frac{2\pi c}{\omega_0}$ = nominal wavelength. (66)

We note that for small angles

$$\cos\psi_{c0}\left(2\tan\alpha_{\max}\right) \approx 2\tan\frac{\theta_a}{2} \approx \theta_a = \text{effective aperture aspect angle in slant plane,} \tag{67}$$

which allows us to describe

$$\rho_x \approx \frac{a_{wx}\lambda_0}{2\theta_a\cos\left(\frac{\theta_{\Delta 0}}{2}\right)}. \tag{68}$$

Some observations

- Clearly, resolutions in both dimensions are coarsened by $\sec\left(\theta_{\Delta 0}/2\right)$. We note that this is a little different than some other derivations.
- The direction of the effective aperture from the MCP is defined by the synthesized unit vector $\mathbf{n}_{c,n}$. All pertinent angles α_n and ψ_n are defined by this synthesized direction.

We state without elaboration that the Doppler shift of an azimuth-offset target reflector with respect to the MCP is calculated as

$$f_D \approx -\Gamma\frac{2}{\lambda_0}s_x\dot{\alpha}, \tag{69}$$

where

$\dot{\alpha}$ = the angular rate that α changes, and
$\Gamma = \begin{cases} +1 & \text{target to right of flightpath} \\ -1 & \text{target to left of flightpath} \end{cases}$. (70)

3.5 Potpourri

Below we briefly discuss some related but ancillary topics.

3.5.1 SAR Image Formation

With precise knowledge of waveforms, timing and control, and TX flight path, the nature of the phase-history data is precisely known, and image formation becomes a deterministic process. Indeed, a matched-filter could be constructed for every pixel in the desired image. Otherwise, more conventional image formation algorithms could be relatively easily adapted to the bistatic image formation processing.[12,13,14,15]

Even with some imperfections in the knowledge of TX motion, timing and control, or waveform characteristics, an autofocus could still be employed.[16]

An interesting phenomenon of bistatic SAR images is that they will often exhibit two shadows; one due to occlusion of TX incident energy, and one due to occlusion of RX echo energy. This is illustrated in Figure 3.

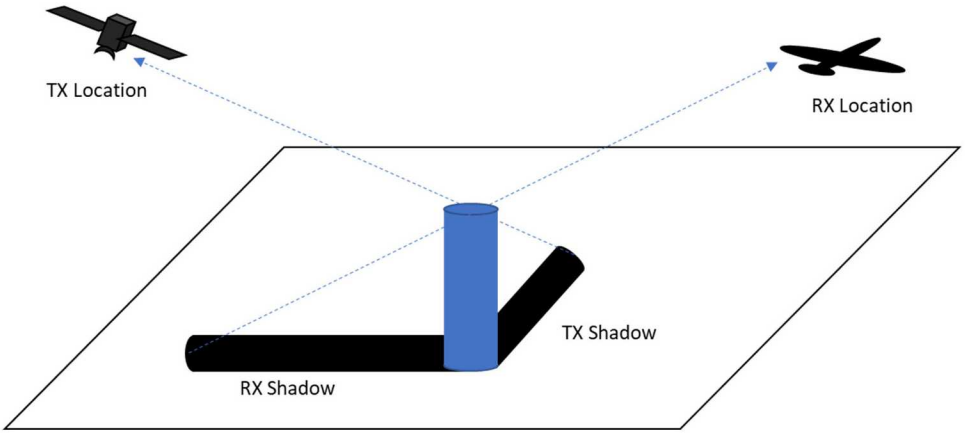

Figure 3. Bistatic SAR images will often exhibit two shadows; one due to occlusion of TX incident energy, and one due to occlusion of RX echo energy.

3.5.2 Polarization

It is well-known that oblique reflections can cause a polarization rotation. Even in the monostatic case, a rotated dihedral is often purposefully used to generate a cross-polarization component to the echo signal.

Never-mind that clutter will itself often have a cross-polarization response, the nature of bistatic radar geometry is that echo reflections are inherently oblique, except for pathological cases. The example in Figure 4 shows how a vertically-polarized transmitted waveform can be received as a horizontally-polarized echo. Furthermore, the amount of polarization rotation of the echo will generally be bistatic geometry dependent.

The implication is that regardless of the polarization of the TX signal, the radar receiver should be fully polarimetric for maximum SNR.

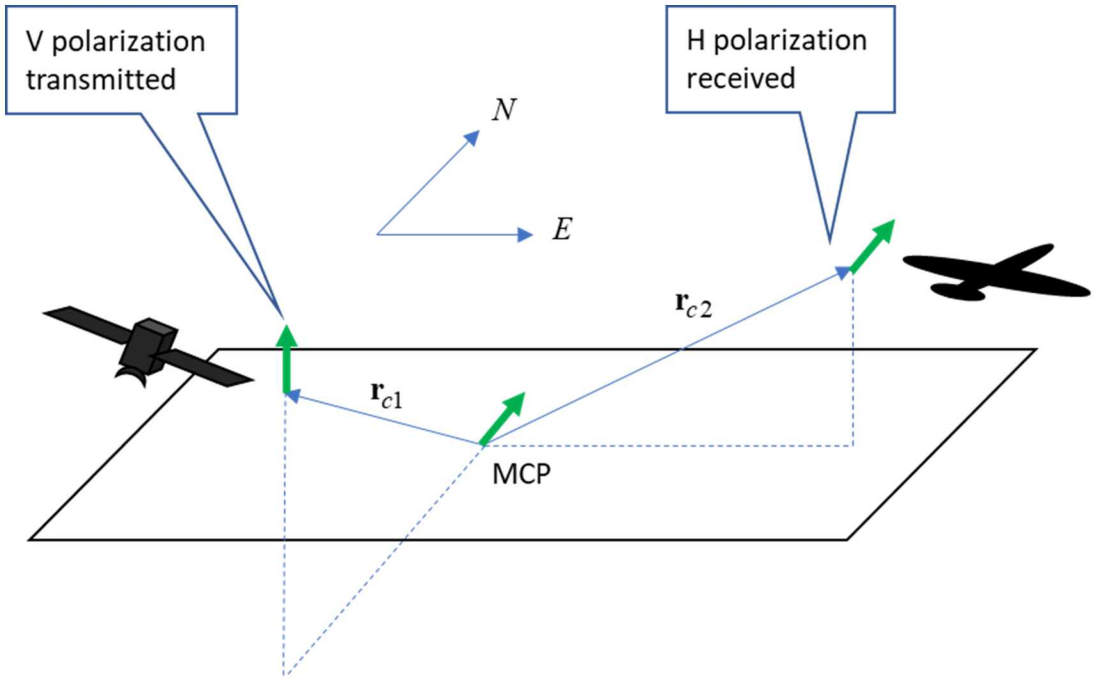

Figure 4. Example: A vertically-polarized TX signal transmitted from south of the MCP will be received as a horizontally-polarized RX signal received east of the MCP. Other bistatic geometries will yield other rotations.

3.5.3 Phase Noise

Phase noise in a master oscillator manifests as clock jitter, which of course manifests as timing jitter. In a monostatic radar system, the phase noise is common to the TX and RX paths, except for a delay. Consequently, in the RX video signal, some parts of the spectrum will coherently add, and other parts will subtract, most especially low-frequency components of the phase noise, which tend to otherwise be at higher levels.[17]

In a bistatic system, where master oscillators of TX and RX systems are different, there will be no cancellation of phase noise spectral regions, generally resulting in higher overall phase noise levels in the echo data.[18]

3.5.4 Test Reflectors

There exists a large body of literature detailing retroreflectors for calibrating and evaluating monostatic radar systems.[19] Being retroreflectors, most of these are unsuitable as general bistatic radar test targets. The list of unsuitable test targets includes the venerable corner reflector. One exception to this list is the spherical canonical reflector.[20]

3.5.5 Ground Moving Target Indicator (GMTI) Radar

Very related to SAR is Ground Moving Target Indicator (GMTI) radar, where conventionally Doppler is assigned to a radial closing velocity of the radar with the moving reflector. As with bistatic SAR, bistatic GMTI can be readily achieved with some adjustments to the relevant equations.

With respect to the earlier development for bistatic SAR, bistatic GMTI also will calculate range and closing velocity with respect to the 'effective' phase center given by Eq. (42) and Figure 2. As a consequence, range resolution will still be governed by Eq. (61) and Eq. (62). However, line-of-sight velocity resolution will now also include the bistatic angle and be given by

$$\rho_v = \frac{a_{wv}\lambda_0}{2\cos\left(\frac{\theta_{\Delta 0}}{2}\right)T_{CPI}}, \tag{71}$$

where

$$\begin{aligned} a_{wv} &= \text{window broadening factor for velocity processing, and} \\ T_{CPI} &= \text{total length of a Coherent Processing Interval (CPI).} \end{aligned} \tag{72}$$

In addition, from Eq. (69) we observe that a stationary target offset in azimuth from the MCP will also generate a relative Doppler offset frequency that depends on the angular rate of the 'effective' phase center. This is responsible for the clutter spread or bandwidth that can obfuscate especially slow-moving targets. The angular rate of the effective phase center depends on, but is not necessarily identically equal to, either the TX velocity or the RX velocity. This can lead to some interesting operational concepts.

For example, forcing the net $\dot{\alpha} = 0$ can collapse the apparent Doppler frequency of stationary clutter to zero (relative to the MCP), thereby minimizing Minimum Detectable Velocity (MDV). This might be accomplished by TX and RX flying counterrotating orbits around a target scene at equal, albeit opposite, angular velocities.[21]

We also note that with the addition of another phase center, whether by one of the radars concurrently operating in a monostatic mode, or a second RX by some other means, then some pathological geometries notwithstanding, we have means of using trilateration for measuring more than just a line-of-sight velocity, such as perhaps additionally a tangential or cross-line-of-sight velocity.

"You can observe a lot by just watching."
-- Yogi Berra

4 Timing and Control (T&C)

For a receiver to optimally form the bistatic SAR image it needs to know several facts about the transmitter. These include

- the TX flight path $\mathbf{r}_{c1,n}$,
- the TX waveform parameters $\phi_{T,n}$, $\omega_{T,n}$, and $\gamma_{T,n}$, and
- the TX pulse reference times t_n and t_0.

The better these are known, the easier is the imaging task.

4.1 Timing Effects on TX Waveform Parameters

The parameters ϕ_T, ω_T, and γ_T, define the TX chirp waveform. Consequently, these parameter values find themselves all over the video signal. Recall from Eq. (14) that

$$\Phi_V = \left\{ \begin{array}{l} -\left[\omega_T + \gamma_T\left(t - t_0 - t_n - t_c\right)\right]\tau_{sc} + \frac{\gamma_T}{2}{\tau_{sc}}^2 \\ +\left[\phi_T - \phi_L + \omega_T\left(\tau_{mc} + \tau_{n'n}\right) + \frac{\gamma_T}{2}\left(\tau_{mc} + \tau_{n'n}\right)^2\right] \\ +\left[\omega_T + \gamma_T\left(\tau_{mc} + \tau_{n'n}\right) - \omega_L\right]\left(t - t_0 - t_{n'} - t_m\right) \\ +\left[\frac{\gamma_T}{2} - \frac{\gamma_L}{2}\right]\left(t - t_0 - t_{n'} - t_m\right)^2 \end{array} \right\}, \tag{73}$$

and (assuming for the moment $\tau_{n'n} = 0$) we require matching the LO parameters such that

$$\begin{aligned} &\phi_L = \phi_T + \omega_T\tau_{mc} + \frac{\gamma_T}{2}{\tau_{mc}}^2, \\ &\omega_L = \omega_T + \gamma_T\tau_{mc}, \text{ and} \\ &\gamma_L = \gamma_T. \end{aligned} \tag{74}$$

Errors in this matching cause undesired phase errors in the phase history data.[22]

In many high-performance SAR systems, the TX waveform is generated by Direct Digital Synthesis (DDS). Consequently, the actual values for these parameters depend on the accuracy of the TX system master clock/oscillator. This implies that the accuracy with which these parameters need to be known sets a limit on clock accuracy (inaccuracy).

Consider the chirp rates. An error in TX chirp rate cancellation will cause a quadratic phase error in range. In a DDS the actual chirp rate is proportional to the square of the system clock

frequency. If the TX system clock frequency is in error by a factor $\left(1+\varepsilon_f\right)$, then a quadratic phase error will result with peak value

$$\phi_{error} = \frac{\pi e_f B_{eff} T_{eff}}{2}. \tag{75}$$

Limiting the peak quadratic phase error to 1 radian and allowing for a 100 μs effective pulse width and a 600 MHz effective bandwidth, the TX clock frequency needs to be kept to within 10.6 ppm of the RX clock frequency. This doesn't seem particularly hard. The spec would get tighter for longer pulses and/or finer range resolutions.

Now consider the waveform center frequencies. An error in the TX center frequency will cause a linear shift in range of the image, but not a misfocus. In a DDS the actual frequency is proportional to the system clock frequency. If the TX system clock frequency is in error by a factor $\left(1+\varepsilon_f\right)$, then a linear phase error will result with peak value

$$\phi_{error} = \frac{e_f \omega_T T_{eff}}{2}. \tag{76}$$

Another way to look at this is as a ranging time delay error given by

$$\tau_{error} = \frac{\phi_{error}}{\omega_T} = \frac{e_f T_{eff}}{2}. \tag{77}$$

The aforementioned 10-ppm TX clock error along with the 100 μs effective pulse leaves us with a ranging error of 0.5 ns, which corresponds to sub-foot range offset. This doesn't seem to be a problem either.

The bottom line is that TX system master clock frequency offsets don't appear to bother waveform parameter precision much until we get to sub-foot resolutions and many tens of microseconds long pulses.

4.2 TX Pulse Reference Time

Our best estimate of the TX pulse reference time t_n is currently $t_{n'}$. We desire these to be the same, which by definition forces $\tau_{n'n} = 0$. Alas, 'tis not always to be. Suppose that our estimate is in error for any of a boatload of reasons, and $\tau_{n'n} \neq 0$.

Recall the phase history model, which after motion compensation and fast-time sampling becomes approximately

$$\Phi_V = \left\{ \begin{array}{l} \frac{2}{c}\left[\omega_0 + \gamma_0 \tau_{n'n} + \gamma_0 T_{s0} i\right] \cos\left(\frac{\theta_{\Delta 0}}{2}\right) \cos\psi_{c0}\left(s_x \tan\alpha_n - s_y\right) + \frac{\gamma_T}{2}\tau_{sc}{}^2 \\ + \left[\left(\omega_T + \gamma_T \tau_{mc}\right)\tau_{n'n} + \frac{\gamma_T}{2}\tau_{n'n}{}^2\right] + \gamma_T \tau_{n'n}\left(t - t_0 - t_{n'} - t_m\right) \end{array} \right\}. \quad (78)$$

Clearly, a reference time error ($\tau_{n'n} \neq 0$) shows up is several places. Two distinct areas are

- LO timing (terms in line 2 of the video phase expression), and
- ADC timing (terms in line 1 of the video phase expression).

To ascertain the effects of this error let us first presume that what we desire is a constant PRF. That is, we desire that

$$t_n = t_{n,nom} + \frac{n}{f_{PRF}}, \quad (79)$$

where

$t_{n,nom}$ = nominal pulse location at center of aperture, and
f_{PRF} = actual PRF of radar. (80)

Now suppose that the presumed values differ from the actual values such

$$t_{n'} = t_{n,nom} + t_\varepsilon + \frac{n}{f_{PRF}\left(1+\varepsilon_f\right)} \approx \left(t_{n,nom} + \frac{n}{f_{PRF}}\right) + \left(t_\varepsilon - \frac{n\varepsilon_f}{f_{PRF}}\right) = t_n + \left(t_\varepsilon - \frac{n\varepsilon_f}{f_{PRF}}\right), \quad (81)$$

where

t_ε = error in presumed pulse reference time at aperture center, and
ε_f = system clock error factor, as previously defined. (82)

From earlier definitions, we equate the timing error

$$\tau_{n'n} = \left(t_\varepsilon - \frac{n\varepsilon_f}{f_{PRF}}\right). \quad (83)$$

Note that this imparts a pulse-to-pulse linear offset characteristic to $\tau_{n'n}$.

4.3 LO Timing Error Effects

Extracting the phase terms from line 2 of the video phase expression in Eq. (78), and inserting the timing error expression yields

$$\Phi_{LO\,error} = \left\{ \begin{array}{l} \left(\omega_T + \gamma_T \tau_{mc}\right)\left(t_\varepsilon - \dfrac{n\varepsilon_f}{f_{PRF}}\right) + \dfrac{\gamma_T}{2}\left(t_\varepsilon - \dfrac{n\varepsilon_f}{f_{PRF}}\right)^2 \\ +\gamma_T\left(t_\varepsilon - \dfrac{n\varepsilon_f}{f_{PRF}}\right)\left(t - t_0 - t_{n'} - t_m\right) \end{array} \right\},$$

$$= \left\{ \begin{array}{l} \left(\omega_T + \gamma_T \tau_{mc}\right)\left(t_\varepsilon - \dfrac{n\varepsilon_f}{f_{PRF}}\right) + \dfrac{\gamma_T}{2}\left(t_\varepsilon{}^2 - 2t_\varepsilon \dfrac{n\varepsilon_f}{f_{PRF}} + \left(\dfrac{n\varepsilon_f}{f_{PRF}}\right)^2\right) \\ +\gamma_T\left(t_\varepsilon - \dfrac{n\varepsilon_f}{f_{PRF}}\right)\left(t - t_0 - t_{n'} - t_m\right) \end{array} \right\},$$

$$= \left\{ \begin{array}{l} \\ \left(\omega_T + \gamma_T \tau_{mc}\right) t_\varepsilon + \dfrac{\gamma_T}{2} t_\varepsilon{}^2 \\ \gamma_T t_\varepsilon \left(t - t_0 - t_{n'} - t_m\right) \\ -\left(\omega_T + \gamma_T \tau_{mc} + \gamma_T t_\varepsilon\right)\dfrac{\varepsilon_f}{f_{PRF}} n \\ -\gamma_T\left(\dfrac{\varepsilon_f}{f_{PRF}}\right) n\left(t - t_0 - t_{n'} - t_m\right) \\ +\dfrac{\gamma_T}{2}\left(\dfrac{\varepsilon_f}{f_{PRF}} n\right)^2 \end{array} \right\}. \tag{84}$$

Of the final expression, line 1 is a constant phase error, which is inconsequential for image formation.

Line 2 represents a video frequency bias which manifests itself as a range shift. The frequency shift is given by

$$\omega_{shift} = \gamma_T t_\varepsilon = \frac{2\pi B_{eff}}{T_{eff}} t_\varepsilon \,. \tag{85}$$

which for $B_{eff} = 600$ MHz, $T_{eff} = 20\,\mu$s, and $t_\varepsilon = 100$ ns, yields a frequency shift of 3 MHz, which is typically a small fraction of a video bandwidth, and not much to worry about too much. The shift will be noticeable, but not completely outside the scene.

Line 3 is a Doppler bias term, which manifests itself as an azimuthal shift of the scene. In many ways it is equivalent to a line-of-sight velocity error. The dominant component of this line is that which contains ω_T. We can compare this Doppler term with that resulting from an azimuthal displacement as

$$\omega_T \left(\frac{\varepsilon_f}{f_{PRF}} \right) n \approx \frac{2}{c} \omega_0 \cos\psi_{c0} \, s_{x,error} \tan\alpha_n . \tag{86}$$

Asserting that

$$\tan\alpha_n \approx \left(\frac{\dot{\alpha}}{f_{PRF}} \right) n , \tag{87}$$

where we recall that

$$\dot{\alpha} = \text{the angular rate that } \alpha \text{ changes,} \tag{88}$$

yields the expression

$$\varepsilon_f \approx \frac{2}{c} \cos\psi_{c0} \, s_{x,error} \dot{\alpha} , \tag{89}$$

which can be solved for an azimuth position offset error

$$s_{x,error} \approx \frac{c\varepsilon_f}{2\cos\psi_{c0} \, \dot{\alpha}} . \tag{90}$$

To gauge the significance of this error term, let us hypothesize $\psi_{c0} = 45^{\circ}$, $s_{x,error} < 100$ m, and $\dot{\alpha}$ consistent with 60 m/s at a range of 10 km. The requirement for oscillator frequency error is $\varepsilon_f < 2.83 \times 10^{-9}$. That is, TX and RX oscillators need to be either matched or compensated to within 2.83 ppb. (Yes, the 'b' stands for billion.) This requires some effort.

Line 4 is a migration term that is not expected to be more severe than line 3.

Line 5 is a quadratic phase error term that will misfocus the image in azimuth, unless compensated. The peak phase error can be calculated as

$$\phi_{error} = \frac{\gamma_T}{2} \left(\frac{\varepsilon_f}{f_{PRF}} n \right)^2 \approx \frac{\pi B_{eff}}{T_{eff}} \varepsilon_f{}^2 \left(\frac{a_{wx} \lambda_0}{2\rho_x \dot{\alpha}} \right)^2 . \tag{91}$$

With $B_{eff} = 600$ MHz, $T_{eff} = 20$ μs, $a_{wx} = 1.2$, $\lambda_0 = 0.02$ m, $\rho_x = 0.3$ m, $\dot{\alpha}$ consistent with 60 m/s at a range of 10 km, and $\varepsilon_f < 2.83 \times 10^{-9}$ as above, the resulting peak quadratic phase error

is calculated to be about 0.005 radians, which is negligible. Even something substantially larger could still be handled easily with an autofocus operation.

The bottom line is that the dominant problem with mismatched TX and LO timing is probably oscillator frequency matching or compensation. Frequency errors need to be controlled or known to within the parts-per-billion range.

4.4 ADC Timing Error Effects

Extracting the appropriate error term from line 1 of the video phase expression in Eq. (78), and inserting the timing error expression into it yields

$$\begin{aligned}\phi_{ADC\ error} &= \left\{\frac{2}{c}\left[\gamma_0\left(t_\varepsilon - \frac{n\varepsilon_f}{f_{PRF}}\right)\right]\cos\left(\frac{\theta_{\Delta 0}}{2}\right)\cos\psi_{c0}\left(s_x\tan\alpha_n - s_y\right)\right\}, \\ &= \left\{\begin{array}{l}\frac{2}{c}\left[\gamma_0 t_\varepsilon\right]\cos\left(\frac{\theta_{\Delta 0}}{2}\right)\cos\psi_{c0}\left(s_x\tan\alpha_n - s_y\right) \\ -\frac{2}{c}\left[\gamma_0\left(\frac{n\varepsilon_f}{f_{PRF}}\right)\right]\cos\left(\frac{\theta_{\Delta 0}}{2}\right)\cos\psi_{c0}\left(s_x\tan\alpha_n - s_y\right)\end{array}\right\}, \\ &= \left\{\begin{array}{l}\frac{2}{c}\left[\gamma_0 t_\varepsilon\right]\cos\left(\frac{\theta_{\Delta 0}}{2}\right)\cos\psi_{c0}\left(s_x\tan\alpha_n - s_y\right) \\ +\frac{2\gamma_0}{c}\cos\left(\frac{\theta_{\Delta 0}}{2}\right)\cos\psi_{c0}\, s_y\left(\frac{\varepsilon_f}{f_{PRF}}\right)n \\ -\frac{2\gamma_0}{c}\cos\left(\frac{\theta_{\Delta 0}}{2}\right)\cos\psi_{c0}\, s_x\left(\frac{\varepsilon_f}{f_{PRF}}\right)n\tan\alpha_n\end{array}\right\}.\end{aligned} \tag{92}$$

Of the final expression, line 1 simply adds a small constant frequency offset to ω_0. As long as we satisfy

$$t_\varepsilon \ll T_{eff}\,, \tag{93}$$

this frequency offset will be of little consequence. This shouldn't be a problem.

Line 2 yields a Doppler offset that is dependent on s_y. This causes a twist in the image. The amount of twist can be calculated by equating this to the legitimate Doppler caused by a true azimuth offset s_x. This comparison is stated as

$$\frac{2\gamma_0}{c}\cos\left(\frac{\theta_{\Delta 0}}{2}\right)\cos\psi_{c0}\, s_y\left(\frac{\varepsilon_f}{f_{PRF}}\right)n = \frac{2\omega_0}{c}\cos\left(\frac{\theta_{\Delta 0}}{2}\right)\cos\psi_{c0}\, s_{x,offset}\tan\alpha_n\,, \tag{94}$$

which can be morphed into the expression

$$s_{x,offset} = \left(\frac{2\pi B_{eff}}{\omega_0}\right)\left(\frac{1}{T_{eff}}\right)\left(\frac{s_y}{\dot{\alpha}}\right)\varepsilon_f \,. \tag{95}$$

As example, at 15 GHz, with $B_{eff} = 600$ MHz, T_{eff} = 20 μs, $\dot{\alpha}$ consistent with 60 m/s at a range of 10 km, s_y = 100 m, and ε_f = 1 ppm, the resulting azimuth shift is 33.3 m. The image centerline would be tilted by about 18.4° in the xy-plane. This would be quite noticeable in the image. Since the azimuth shift scales directly with ε_f, reducing ε_f to 10 ppb would reduce the azimuth shift to a barely noticeable 0.33 m.

Line 3 yields essentially an azimuth position dependent quadratic phase error with peak value approximately

$$\begin{aligned}\phi_{error} &\approx \frac{2\gamma_0}{c}\cos\left(\frac{\theta_{\Delta 0}}{2}\right)\cos\psi_{c0}\, s_x\left(\frac{\varepsilon_f}{f_{PRF}}\right)\left(\frac{N}{2}\right)\tan\alpha_{\max}\,, \\ &\approx \left(\frac{\lambda_0^2}{c}\right)\left(\frac{2\pi B_{eff}}{T_{eff}}\right)\left(\frac{1}{8}\right)s_x\left(\frac{a_{wx}}{\rho_x}\right)^2\left(\frac{1}{\cos\left(\frac{\theta_{\Delta 0}}{2}\right)\cos\psi_{c0}}\right)\left(\frac{1}{\dot{\alpha}}\right)\varepsilon_f \,.\end{aligned} \tag{96}$$

At 15 GHz, with $B_{eff} = 600$ MHz, T_{eff} = 20 μs, s_x = 100 m, a_{wx} = 1.2, ρ_x = 0.3 m, $\theta_{\Delta 0} = 90°$, ψ_{c0} = 45°, $\dot{\alpha}$ consistent with 60 m/s at a range of 10 km, and ε_f = 1 ppm, the peak quadratic phase error reaches 4.2 radians, or 240°. By limiting ε_f to 10 ppb, the peak quadratic phase error is reduced to an unnoticeable 2.4°.

The bottom line is that for spatially-variant quadratic phase errors and image twist to be negligible, the TX and RX master clock/oscillators need to be compensated to within the low parts-per-billion range.

4.5 Combined Results

Primarily due to LO timing error effects, the mean timing error t_ε should probably be kept to within 100 ns, preferably in the 10 ns range.

Also, primarily due to LO timing error effects, the master clock/oscillator frequencies need to be matched or compensated to within single-digits parts-per-billion, preferably in the neighborhood of 1 ppb.

These numbers are consistent with the literature.[23]

4.6 Relativistic Effects

Both special relativity and general relativity begin to show their influence if one or the other of the TX and RX are in orbit around the earth. We do note that GPS system clocks are adjusted to compensate for relativistic effects, including general relativity relativistic effects.[24] Consider the case of the TX on a satellite in orbit and the RX in an airborne vehicle.

4.6.1 Special Relativity

From special relativity, we understand that when bodies exhibit a relative velocity with respect to each other, time dilation occurs, which affects relative frequency measurements. Time slows down for the observer, and as time slows down, so do clocks and oscillators.[25]

For example, consider the RX to be in the reference inertial frame, with the TX exhibiting a relative velocity with magnitude v_{TR}. To an observer at the RX location, time increments at the TX will appear to have lengthened, causing a reduction in observed frequency by a factor

$$\omega_{RX\,observed} = \omega_{TX\,frame}\sqrt{1-\left(\frac{v_{TR}}{c}\right)^2}\,. \tag{97}$$

For normal terrestrial velocities, this is inconsequential. For example, if v_{TR} = 300 m/s, the time dilation accounts for a frequency change of about –0.0005 ppb. However, with the TX in low-earth orbit, with perhaps v_{TR} = 7400 m/s, then the frequency change corresponds to –0.3 ppb. While not terribly large in comparison to our examples, it nevertheless approaches the magnitude of the error limit we desire.

4.6.2 General Relativity

From general relativity, we understand that a photon traveling from a higher gravitational potential to a lower gravitational potential will exhibit a change in its frequency to account for its energy gain. This is the same phenomenon that leads to gravitational red-shift, gravity lenses, and black holes. Specifically, the ratio of frequencies becomes

$$\omega_{RX\,observed} = \omega_{TX\,frame}\left(1-\frac{GM}{c^2 r_1}\right)\Bigg/\left(1-\frac{GM}{c^2 r_2}\right). \tag{98}$$

where

G = 6.673231 x 10^{-11} Nm^2/kg^2 = universal gravitational constant,
M = 5.979 x 10^{24} kg = mass of the earth,
r_1 = initial (TX) radial distance from mass center, and
r_2 = final (RX) radial distance from mass center. (99)

It is understood that these radii are both greater than the radius of the earth, which averages about 6.371315 x 10^6 m.

For atmospheric vehicles this tends to be negligible. For example, with the TX at 65 kft above the RX at the mean earth radius, the TX frequency will increase by 0.00216 ppb. However, with the TX in low-earth orbit, say at 400 km above the RX at mean earth radius, the TX frequency will increase by 0.0412 ppb. From a more GPS-like altitude of 2100 km, the frequency shift will be more like 0.535 ppb. This is starting to become noteworthy.

4.6.3 Combined Relativistic Effects

We note that for an orbiting TX, the RX will perhaps see effects due to both special and general relativity. Furthermore, for an orbiting TX, these effects will pull frequencies in opposite directions. The combined effects can be seen in the following figure due to circular orbits out to geosynchronous altitudes. Note that depending on altitude, the net shift can be either positive or negative, and perhaps even zero.

The bottom line is that if we begin to consider a partially space-based system, and if we begin to require better than 1 ppb clock accuracy, then we need to begin to consider relativistic effects. Otherwise we don't. For the moment, we don't.

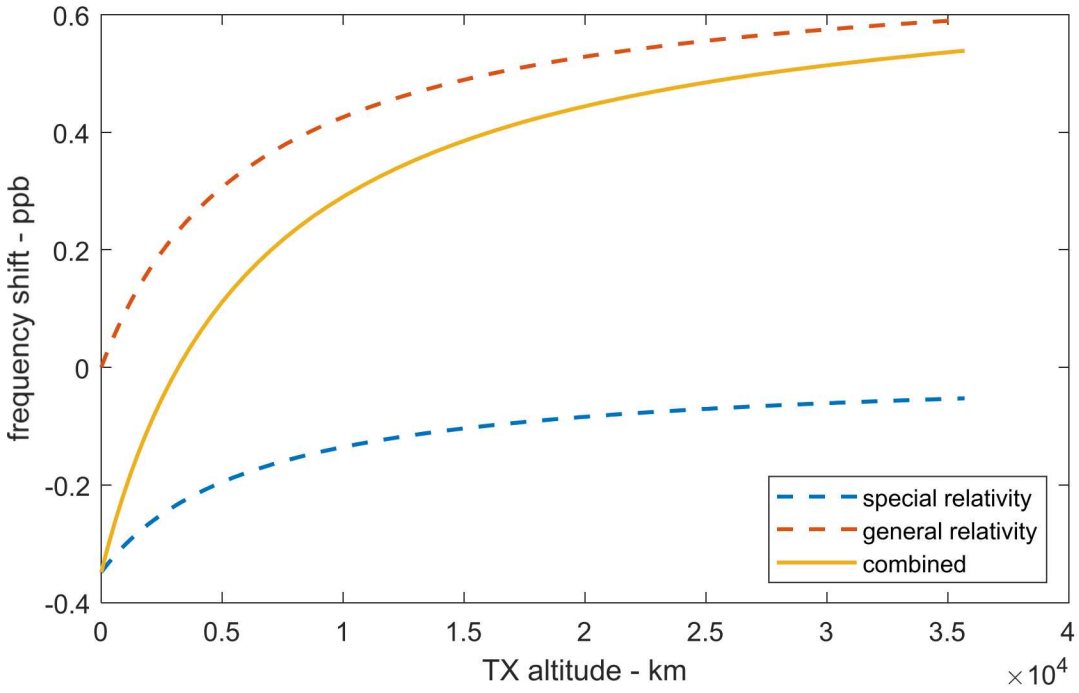

Figure 5. Relativistic effects due to orbiting TX.

“Progress is man's ability to complicate simplicity.”
-- Thor Heyerdahl

5 Synchronizing RX to TX

As previously noted, for a receiver to optimally form the bistatic SAR image it needs to acquire the following parameters of the transmitter.

- the TX flight path $\mathbf{r}_{c1,n}$, actually the TX positions when pulses were emitted,
- the TX waveform parameters $\phi_{T,n}$, $\omega_{T,n}$, and $\gamma_{T,n}$, and
- the TX pulse reference times t_n and t_0.

5.1 Acquiring TX Motion

A notion of the location of the transmitter during the data collection pass is crucial to forming high-quality bistatic SAR images. Recall that even if the TX waveform parameters are known exactly, the phase history for pulse *n* is described from Eq. (46) as

$$\Phi_V(i,n) = \left\{ \frac{2}{c} \left[\omega_{T,n} + \gamma_{T,n} \left(\tau_{n'n} + t_{ADC,n} + iT_{s,n} - t_{c,n} \right) \right] \cos\left(\frac{\theta_{\Delta,n}}{2} \right) \left(\mathbf{n}_{c,n} \bullet \mathbf{s} \right) \right\}. \tag{100}$$

Even in this ideal model, the parameters $t_{c,n}$, $\theta_{\Delta,n}$, and $\mathbf{n}_{c,n}$ explicitly depend on the TX position for each pulse, and hence motion. In fact, knowing the very resolution of a particular data set depends on the effective aperture, which in turn depends on TX geometry and motion.

Consequently, the TX motion during a data collection is a vital piece of information for the RX to have. As with the waveform parameters, the following qualitatively described techniques do not form an exhaustive list.

A tacit assumption here is that the TX is in fact illuminating the scene which the RX intends to image. That is, both TX and RX antennas are being pointed to the region of the desired MCP.

5.1.1 Stationary TX

The simplest scheme for the RX to know the TX motion is for the TX to remain at a location exactly known to the RX. This might be at a fixed (stationary) location, such as a tower or mountain-top peak. Geosynchronous orbit might suffice. In any case, the TX motion is known a priori to the RX.

A variant of this is for the TX to be located at a point fixed relative in some manner to the RX, such as another part of the aircraft. The motion of the TX is readily accessible to the RX, or at least easily measured.

In either case, no platform-to-platform communication is required, beyond perhaps mission planning.

5.1.2 Predictable Flight Path

The next simplest scheme is for the TX motion to be adequately predictable to the RX. An example might be the TX carried by a satellite in a precisely known, predictable orbit. This works for GPS, so it seems like it might work for a bistatic SAR system, too.

As with the stationary TX, no platform-to-platform communication is required, at least during the data collection pass. Mission planning would dictate when the RX might collect usable data, and perhaps incorporate the latest satellite orbital data.

5.1.3 Ancillary Data Signal

In the event that the TX flight path is not suitably predictable, such as perhaps with an airborne TX, then the actual flight path needs to be discernible in some manner to the RX during a data collection pass. The easiest way to do this is for a friendly TX to communicate its motion to the RX, perhaps in an ancillary data path or channel.

As was discussed with TX waveform parameters, it might be possible to attach the motion data in some manner to the TX signal itself. An interesting variant of this idea is for the TX waveform to be a spread-spectrum pseudo-noise sequence (instead of an LFM chirp), where the motion data is encoded into (and hence becoming a part of) the actual transmitted waveform. Think of using a high-power, wide-band, GPS-like signal as the transmitted waveform.

5.1.4 Direct Observation

For an unfriendly TX (that does not help the RX by providing its motion data), the RX must attempt to discern what it can about the TX motion. For example, a third tracking radar might monitor TX motion and relay the information to the RX.

Or perhaps the direct-path TX signal could be monitored by the RX employing a separate (from the radar RX antenna) dual-axis monopulse antenna. This would yield angle-angle measurements of the TX position relative to the RX position. A priori knowledge of pulse timing might help in providing relative range to the TX, for a full 3-D motion solution.

5.1.5 Autofocus

The RX collected phase history data will exhibit degradation from imprecise knowledge of the TX (and RX) flight paths. The dominant effect is expected to be an image scene-wide common phase error due to imprecise knowledge of $|\mathbf{r}_c|$. If the data is 'close' (without defining 'how close') then the common phase error can be estimated from the image itself, and used to filter the image to a focused condition. This is routinely done for fine resolution monostatic SAR images. Typical monostatic SAR image formation implementations might employ a Phase-Gradient Autofocus (PGA) algorithm,[26] which is expected to provide the same benefit to bistatic SAR imaging.

However, the initial phase history data (prior to autofocus) needs to at least contain the echoes of the scene to be imaged. This means that autofocus can only work on data that is already

sufficiently 'in the ballpark', and being in the ballpark, in turn, requires at least some knowledge of TX motion during the data collection (as well as TX antenna pointing).

Schemes do exist to keep otherwise 'sloppy' SAR systems collecting data from a fixed region on the ground. These fall under the general heading of "Clutter-Locking." These techniques can be used by bistatic SAR systems to adjust RX timing and LO waveform parameters to accommodate otherwise unsensed motion. But clutter-locking can sometimes cause strange behavior in SAR systems, by tending to lock onto brighter targets, and perhaps shifting its focus during an aperture. In any case, clutter-locking also works best when a priori assumptions can be made of the unsensed motion, like there being considerable correlation from one pulse to the next.

It remains unclear at this time how to estimate other aspects of TX motion, such as those involved with calculating bistatic angle $\theta_{\Delta,n}$, and the direction of the effective phase centers $\mathbf{n}_{c,n}$, with some sort of autofocus operation.

5.2 Acquiring TX Waveform Parameters

Recall from Eq. (74) that the proper LO waveform (in the sense of deriving the desired phase history model with minimal phase perturbations) requires

$$\begin{aligned} \phi_L &= \phi_T + \omega_T \tau_{mc} + \frac{\gamma_T}{2} \tau_{mc}^2 , \\ \omega_L &= \omega_T + \gamma_T \tau_{mc} , \text{ and} \\ \gamma_L &= \gamma_T . \end{aligned} \tag{101}$$

Furthermore, image resolution also requires knowledge of the TX waveform parameters. Errors in the presumption of the TX parameters ultimately lead to image target displacements and misfocusing. Consequently, for optimal image formation, we require precise values for these parameters.

The question is "How do we get precise values for these parameters from the TX to the RX?"

The following techniques are briefly described in a qualitative sense. These are not meant to form an exhaustive list of techniques.

5.2.1 A Priori Knowledge

This simplest scheme for making the RX aware of TX waveform parameters is for the TX to use previously agreed upon constant values for these parameters. While this requires some coordination prior to a mission, and a friendly TX, it nevertheless doesn't require communication between TX and RX during a data collection pass or mission.

This does place a greater burden on the RX, by requiring it to perform any real-time motion compensation using the LO, but "So what?", we know how to do that.

5.2.2 Ancillary Data Signal

An alternative to performing the requisite waveform coordination prior to a mission is to perform the coordination 'in-flight'. This would require a communication from the friendly TX to the RX by some data path or channel perhaps in addition to the actual transmitted signal.

A variant of this might be a third party controlling (and communicating to) both the TX and RX to force this coordination.

Another variant might be to attach the parameter values as 'data' to the actual transmitted waveform in some manner, perhaps as a phase modulation to the trailing end of the chirped pulse. A similar notion has been explored for radar transponder tags.

5.2.3 Direct Observation

In the absence of the TX sharing 'data" on its waveform properties with the RX, the RX must determine what it needs to know from the raw radar signal itself. The success of this scheme depends on the ability of the RX to extract the required information. This depends heavily on Signal-to-Noise (SNR) and the correctness of any presumptions the RX makes about the TX signal.

For example, if the RX has access to a direct line-of-sight signal from the TX (perhaps through a TX sidelobe), then a reasonable SNR might be had. If relative Doppler is properly accounted for, the signal processing might provide a reasonable estimate of TX chirp-rate and center frequency. If these (as well as reference phase) can be presumed to be constant from pulse to pulse, then this becomes a relatively easy exercise in parameter estimation.

If the direct signal is not available, or good enough, then the parameters might need to be estimated from the scene reflections themselves. This is a harder problem. It is precisely a parametric 'autofocus' problem, but in the range dimension instead of the more usual azimuth dimension. As with any autofocus, this 'range-autofocus' operation works better the closer everything starts to being in focus in the first place. That is, even a poor initial parameter guess is probably better than no guess at all. From a practical standpoint, for fine resolution image formation using stretch processing, the receiver must do a good enough job of de-ramping the received pulses to fit the information through the Intermediate Frequency (IF) filters.

Countermeasures

The underlying presumption to estimating pulse parameters is that the relationship of these parameters from pulse to pulse is adequately known to the receiver. If this presumption is invalid, say by the TX perhaps purposely employing pulse-to-pulse random phase coding, then this renders the RX data 'screwed-up' and likely unusable (or at the very least makes the RX's job much, much harder).

The only real recourse is for the RX to sample the direct TX signal in some manner and use it as the matched filter for the scene echoes. This can be done either in whole or in part. For example, we might sample the entire full-bandwidth TX signal and use it to match-filter the full-bandwidth

echoes, or we might partially deramp the TX LFM chirp signal before sampling and use it to match-filter the partially-deramped echoes.

Of course, if we sample the full bandwidth TX signal for a matched filter, we are no longer really limited to LFM chirps, or even dedicated radar transmitters. Transmitters of opportunity, such as broadcast transmitters, might be employed.[27,28] Of course, resolution is still limited by bandwidth.

5.3 Synchronization of TX and RX Timing

There are two major timing synchronization issues that need to be addressed and solved.

- The RX needs to determine the TX's relative master clock/oscillator frequency to within a precision of under 10 ppb (preferably to 1 ppb), in some scenarios.

- The RX needs to determine the TX's pulse timing reference to within about 100 ns (preferably 10 ns), with any 'drift' constrained to the same 10 ppb (preferably 1 ppb) as the master clock.

Several schemes are presented in the literature.[29,30,31]

5.3.1 Master Clock/Oscillator Frequency Synchronization

The most obvious solution to synchronizing the TX and RX master clock/oscillator is to ensure that the TX and RX system clock frequencies are as frequency-locked as possible, perhaps by tuning them actively against each other, or a third standard such as GPS.

A better scheme might be to measure the TX and RX frequency offsets as accurately as possible, perhaps against GPS, and accounting for them in RX timing equations. All we really need to know is the TX clock frequency error with respect to the RX clock, that is, we ask the question "If the TX is providing signals based on what it thinks is a 100 MHz reference, what would the RX measure the reference to be?"

Several schemes to effectively synchronize TX and RX oscillators are discussed below. We note that what needs to be synchronized (or compensated) are the TX and RX master clock frequencies, and not their phases. That is, we're looking for frequency-lock, not phase-lock.

5.3.1.1 Get better clock/oscillators

Oddly enough, frequency standards with part-per-billion accuracies and precisions do exist. For example, cesium or hydrogen maser class clocks exhibit on the order of 0.001 ppb stability over years. These tend to be expensive, however, at prices in the range of $60k at the time of this writing. While perhaps expensive compared to other clock sources, this typically would be nowhere near the most expensive sub-system in a high-performance SAR system. Lesser technologies and options also exist.

5.3.1.2 Direct frequency measurement

Consider the RX actually measuring a calibration signal synchronous with TX reference clock frequency. The error is then calculated to be

$$\varepsilon_f = \frac{f_{c,TX}}{f_{c,RX}} - 1 \tag{102}$$

where

$$\begin{aligned} f_{c,TX} &= \text{TX calibration frequency, and} \\ f_{c,RX} &= \text{RX calibration frequency.} \end{aligned} \tag{103}$$

The trick is to get a sample of $f_{c,TX}$ over to the RX. A calibration tone could be transmitted from the TX to the RX, but any Doppler would then have to be accounted for. The question becomes "Can TX and RX motion be measured accurately enough to predict and remove Doppler well enough from the TX reference tone?"

Another question might be "Can the direct path of the TX signal be used in this manner?"[32]

5.3.1.3 Frequency measurement and calibration against a third standard

If a direct measurement can't be made, perhaps the TX and RX can each make independent and separate measurements of their own clock frequencies, and correct their waveform and timing accordingly.

Suppose there exists a separate known reference clock frequency observable to both the TX and RX (e.g. perhaps GPS carrier frequency measurements). The TX would measure its own error against this standard by

$$\varepsilon_{f,TX} = \frac{f_{c,ref}}{f_{c,TX}} - 1, \tag{104}$$

and correct its signals to the standard.

The RX would do the same, so that it calculates

$$\varepsilon_{f,RX} = \frac{f_{c,ref}}{f_{c,RX}} - 1. \tag{105}$$

If the TX corrects its own waveform and timing, then

$$\varepsilon_f = \varepsilon_{f,RX}. \tag{106}$$

If the TX did not correct its own waveforms, then the corrections would need to be folded into the RX waveform and timing calculations. Effectively, then

$$\varepsilon_f = \frac{\varepsilon_{f,RX}+1}{\varepsilon_{f,TX}+1} - 1 \approx \varepsilon_{f,RX} - \varepsilon_{f,TX} . \tag{107}$$

Anecdotal experiments seem to support this concept as viable.

At the time of this writing, airborne-qualified Rubidium source oscillators are available with about 10^{-10} accuracy and stability.†

GPS receivers on the market have been shown to offer a reference clock with as good as 0.001 ppb accuracy and 0.01 ppb stability.[33]

5.3.1.4 *Image Shift Measurements*

Recall that a clock offset looks like an unaccounted-for line-of-sight velocity, that is, a Doppler bias. We desire to place zero-Doppler in the center of the RX antenna beam. We know that ε_f shifts zero-Doppler to someplace other than where the antenna is pointed, and that the shift is calculated to be

$$s_{x,error} = \frac{c\varepsilon_f}{2\cos\psi_{c0}\dot{\alpha}} . \tag{108}$$

If the difference between antenna beam-center and zero-Doppler could be measured, then clock frequency error could be calculated as

$$\varepsilon_f = (2/c)\cos\psi_{c0} s_{x,error}\dot{\alpha} . \tag{109}$$

This would be facilitated by increasing PRF so that the RX antenna pattern were clearly visible and measurable. Of course, the TX antenna pattern might get in the way.

This is similar to Clutter-Locking, except that the adjustment is to the estimate of ε_f.

5.3.2 Pulse Reference Time Synchronization

The idea here is for the RX to estimate as precisely as possible the TX pulse reference time t_n. This would force the error term $\tau_{n'n}$ to zero. This task is substantially assisted by first synchronizing the TX and RX master clock/oscillator frequencies, as described in the previous section.

---

† E.g. Orolia Spectratime LPFRS/AV1 Airborne Rubidium Oscillator, https://www.orolia.com/products/atomic-clocks-oscillators/lpfrsav1-airborne-rubidium-oscillator.

An ambivalent TX has no knowledge of the RX position or motion. Consequently, it also has no knowledge of the effective phase center position or effective aperture. Therefore, the TX is unable to optimally place the spatial sample points along the effective synthetic aperture. The best that the TX can do is emit its signal at times either communicated to, or predictable to, the RX. This is easiest achieved by fixing the PRF to a constant value known to the RX.

In any case, several schemes to effectively synchronize TX and RX pulse reference times are discussed below. Recall that we desire this error to be within 100 ns (preferably 10 ns), with any drift rate known to within 10 ppb (preferably 1 ppb).

5.3.2.1 Measurement of the TX pulse

Consider a pulse transmitted with center at time $(t_n + t_0)$. It arrives at the RX via the direct (TX to RX line-of-sight) path at time

$$t_{RX\ direct\ path} = (t_n + t_0) + \frac{|\mathbf{r}_{c1} - \mathbf{r}_{c2}|}{c}. \tag{110}$$

Consequently, the RX can set its pulse time reference to

$$t_{n'} = t_{RX\ direct\ path} - t_0 - \frac{|\mathbf{r}_{c1} - \mathbf{r}_{c2}|}{c}. \tag{111}$$

If the direct path signal is a chirp, then the RX can in fact de-chirp the signal to get very accurate time measurements. Some provision might need to be made to estimate the contribution of Doppler to this estimate.

We note that this scheme does have some ability to deal with non-constant, or unknown PRF.

5.3.2.2 Measurement of a third standard

For unambiguous determination of t_n, the TX can synchronize t_n with some other observable event (by the RX) that occurs at a submultiple of the PRF. For example, if the PRF were 1 kHz, then a 1 Hz event observable to both the TX and the RX might be used.

GPS receivers on the market have been shown to offer such a timing mark with as good as 10 ns accuracy.[33]

5.3.3 Correcting the TX signal for clock error

Since timing is typically quantized to some convenient step size (often several nanoseconds at the time of this writing) the question exists "How do we get a precise PRF from the TX if its timing is off?" In other words, "How do we get a PRF that corresponds to a nonintegral number of basic timing steps?"

Recall from Eq. (2) that we want to transmit a pulse with phase given by

$$\Phi_{TX} = \phi_T + \omega_T\left(t - t_0 - t_n\right) + \frac{\gamma_T}{2}\left(t - t_0 - t_n\right)^2 . \tag{112}$$

We presume that the pulse length is long enough to yield the chirp bandwidth desired, account for the range-swath desired, and account for any timing offsets and errors that might be expected. Let us presume also that we desire a fixed PRF such that

$$t_n = \frac{n}{f_{PRF}} = nT_{PRI} . \tag{113}$$

where $T_{PRI} = 1/f_{PRF}$ = the desired constant pulse period (PRI).

Now let us suppose that the radar has a system clock that is quantized in time to an arbitrary but precisely known period T_K where $T_K \ll T_{PRI}$. The PRI is then established by counting the appropriate number of periods T_K. This is just about how every modern radar works. However, since T_{PRI} may not be a multiple of T_K, we need to account for this.

Consider the following. Suppose we establish

$$K_n = \text{round}\left(T_{PRI}/T_K\right) = \text{timer count for the nth pulse,} \tag{114}$$

so that

$$T_{PRI} = K_n T_K + \tau_{PK} , \tag{115}$$

where τ_{PK} is a timing error term. We therewith establish that

$$t_n = n\left(K_n T_K + \tau_{PK}\right) = nK_n T_K + n\tau_{PK} . \tag{116}$$

where $n\tau_{PK}$ represents a linearly growing error term in the times of t_n. This is not good, since even if we adjust the phase of the TX signal to accommodate the phase changes, the pulse envelope will eventually slip excessively. Note, however, that this slip is entirely predictable.

Now consider that we incorporate the past errors into the timer-count calculation so that

$$K_n = \text{round}\left(\frac{T_{PRI} + \tau_{PK,n-1}}{T_K}\right) = \text{new timer count for the nth pulse, and}$$
$$\tau_{PK,n} = T_{PRI} + \tau_{PK,n-1} - K_n T_K \ . \tag{117}$$

Consequently,

$$t_n = \sum_i^n \left[K_i T_K\right] + \tau_{PK,n} , \tag{118}$$

with the error bounded to $\pm T_K/2$. The TX phase thereby becomes

$$\Phi_{TX} = \phi_T + \omega_T\left(t - t_0 - \sum_i^n [K_i T_K] - \tau_{PK,n}\right) + \frac{\gamma_T}{2}\left(t - t_0 - \sum_i^n [K_i T_K] - \tau_{PK,n}\right)^2 , \qquad (119)$$

which can be manipulated to

$$\Phi_{TX} = \left\{ \begin{array}{l} \phi_T - \omega_T \tau_{PK,n} + \frac{\gamma_T}{2}{\tau_{PK,n}}^2 \\ \left(\omega_T - \gamma_T \tau_{PK,n}\right)\left(t - t_0 - \sum_i^n [K_i T_K]\right) \\ + \frac{\gamma_T}{2}\left(t - t_0 - \sum_i^n [K_i T_K]\right)^2 \end{array} \right\} , \qquad (120)$$

From this we can clearly see that if the TX centers its pulses at the quantized times

$$t_{TX\ pulse center} = t_0 + \sum_i^n [K_i T_K] , \qquad (121)$$

and furthermore adjusts its reference phase and frequency to

$$\begin{aligned} \phi'_T &= \phi_T - \omega_T \tau_{PK,n} + \frac{\gamma_T}{2}{\tau_{PK,n}}^2 \text{ , and} \\ \omega'_T &= \omega_T - \gamma_T \tau_{PK,n} , \end{aligned} \qquad (122)$$

then the reference chirp parameters ϕ_T, ω_T, and γ_T will all be properly achieved at the desired times $(t_n + t_0)$. Any error in t_0 is small and constant, therefore of little consequence. Except for the actual pulse start and stop times, the RX won't know, and won't care, what the TX true clock period T_K really is. The actual period T_K has been made irrelevant to the PRF.

If, furthermore, ω_T and γ_T are themselves compensated for the true clock period T_K, then the RX may presume that $\varepsilon_{f,TX} = 0$.

As for pulse start and stop times, if some third party sync signal like GPS is used to estimate $t_{n'}$, then the actual pulse width is also irrelevant, as long as it is long enough. This is very analogous to how and why the receiver derives the parameter τ_{mc}.

5.3.4 Summary on Timing Synchronization Techniques

Especially with the availability of GPS, this looks quite doable.

Probably the best overall solution for frequency locking the TX and RX master clocks is to modify the master clocks of the two systems to be electrically tunable, and to measure their output frequency against GPS. Each error is then mitigated by electrically tuning the respective Stable Local Oscillator (STALO) reference oscillator. This would be a background periodic automatic calibration operation.

Pulse timing would reference the GPS timing marks.

5.3.5 Dealing with a Sub-optimal PRF

Optimal phase history data collection requires that pulses be transmitted at precise angles defined by the synthetic direction unit vector $|\mathbf{n}_c|$. LO and ADC timing depend on $|\mathbf{r}_c|$. Of course these angles and timing depend on both the TX and RX flight geometries. Since the TX is ambivalent (has no knowledge of RX position), this is clearly not possible. The best we can do is have the TX transmit at precise times without regard for RX geometry. Consequently, there will likely exist errors in the optimal placement of the effective aperture.

Given good data on TX motion, as well as its own motion, the RX can interpolate the collected phase history data to the correct spatial positions. In the absence of good motion data, even the corrected data will contain residual improper spatial placement. That is, the data will be corrected to the wrong places.

Placement errors in the direction of the MCP will generate phase errors that are more-or-less common across the entire image, and can be mitigated by traditional autofocus algorithms.

Placement errors in the along-track direction will cause spatially variant phase errors, that is, phase errors that vary across an image, in this case with an odd symmetry in azimuth. No autofocus algorithm currently exists to mitigate this.

Along-Track Autofocus

The manifestation of along-track position errors in SAR phase history data is an image with progressively worse azimuth sidelobes as azimuth distance from the focal point increases. This suggests that an autofocus algorithm that was sensitive to azimuth position might mitigate the azimuth dependent smearing. Subaperture image formation algorithms such as Overlapped-Subaperture (OSA) naturally break an image into many azimuth-mosaicked sub-images.[34] Consequently it seems reasonable to autofocus each sub-image independently. In subaperture language, this means that each azimuth coarse-resolution bin receives its own autofocus treatment, by something like a Phase-Gradient Autofocus (PGA) algorithm.‡

‡ Experiments validate this idea.

5.4 Summary of TX Data Required by RX

For the RX to optimally form bistatic SAR images, it needs to know some things about the TX. What the RX doesn't know, it needs to guess at however it can.

We divide the required parameters into the following categories.

TX motion

The RX needs to know where the TX is. In this report this corresponds to the vector $\mathbf{r}_{c,1}$. Furthermore, it would be most useful for the RX to know the time behavior of the vector $\mathbf{r}_{c,1}$, that is, the pulse-to-pulse updated velocity vector of the TX.

TX pulse waveform parameters.

The RX needs to know TX phase, frequency, and chirp rate. In this report, this corresponds to ϕ_T, ω_T, and γ_T.

We note that the TX phase really only needs to be explicitly known as a function of pulse number *n*. That is, the RX needs to be aware of any particular phase-coding employed by the TX, otherwise absolute phase is not required.

TX timing

The RX needs to know the basic timing of the TX. That is the RX needs to have a sense of what time means to the TX. This includes the underlying time-scale differences in the TX relative to the RX, which in this report is the clock-frequency error ε_f. Furthermore, the RX needs to know the TX pulse-to-pulse reference times, which in this report includes t_n, t_0, and the PRF.

We note that parameters such as the TX pulse length would also be most useful.

With the proper information available to the RX, SAR image formation is no less deterministic in a bistatic SAR than for a monostatic SAR.

In the absence of this information, some estimate of these parameters needs to be made, perhaps augmented by additional signal measurements, and additional signal processing.

6 Notional Bistatic SAR System Characteristics

In this section we present two notional descriptions of separate bistatic SAR systems. To facilitate high-quality, fine-resolution, and reliable bistatic SAR images at minimal cost, we first propose a Class 2 bistatic SAR (friendly but ambivalent TX). The second system uses a spaceborne transmitter and airborne receiver in a Class 3 bistatic SAR system.

6.1 Notional Bistatic SAR System 1 - Airborne TX

6.1.1 TX Waveform Parameters

This first Notional Bistatic SAR System (NBSS-1) would employ a transmitter with constant TX waveform parameters. That is, chirp-rate and center frequency would be constant, as well as pulse length and PRF, and known to the RX.

The TX reference phase might employ random phase encoding to mitigate range ambiguities, and deny an adversary the use of the TX in a bistatic fashion. The random phase code would be calculable by the RX from a seed down-loaded prior to the data collection mission.

System Implications

Real-time motion compensation will require the modulation of ADC start time and sample-spacing. These will have to be adapted to the TX geometry on a pulse-to-pulse basis. This may require adding parameter automatic update registers to the ADC strobe circuitry.

The PRF constraints will likely require the development and implementation of an along track autofocus algorithm.

6.1.2 TX Motion Measurement

The TX is already conspicuous to an RF observer, so there is no point in trying to hide it. Consequently, nothing is lost by adding a second transmitter to the same vehicle to broadcast TX location and motion data. The NBSS-1 would employ such a separate data channel to broadcast TX location and motion data to all RXs in the neighborhood. This data would also include where the TX antenna beam is pointed. This data could be encrypted to deny it to an adversary.

This data channel should have hooks to allow transmission of TX waveform parameters to the RX, to facilitate operating mode changes such as resolution, etc.

System Implications

The effective phase center parameters (and ultimately the effective aperture) will be calculated in the RX. We note that the effective phase center will exhibit motion different than either the TX or RX by themselves. Consequently, coordinate frames for the NBSS-1 likely need to be decoupled from TX and RX vehicles.

Traditional autofocus will also be employed, perhaps as a part of the yet-to-be-developed along-track autofocus algorithm.

Clutter-locking is not expected to be necessary with the employment of the data channel.

6.1.3 Timing and Synchronization

The NBSS-1 proposes to employ electrically tunable STALO master oscillators in both the TX and RX. These would both be frequency locked to GPS, and hence to each other. Furthermore, the PRF of the TX would be held constant, and locked to a GPS timing mark.

System Implications

The RX will assume perfect TX timing, that is, the TX is locked to GPS. This, of course, implies that suitable GPS performance (e.g. P(Y) code, or equivalent) is available to both the TX and RX of the NBSS-1.

6.2 Notional Bistatic SAR System 2 - Spaceborne TX

6.2.1 TX Waveform Parameters

This second Notional Bistatic SAR System (NBSS-2) would employ a spaceborne transmitter of opportunity with presumed constant TX waveform parameters. That is, chirp-rate, center frequency, and starting phase would be presumed to be constant, as well as pulse length and PRF.

System Implications

The RX would need to measure the TX waveform parameters in some fashion, prior to collecting phase history data for image formation. It would do so using the direct-path signal from a roof-mounted antenna.

As with NBSS-1, real-time motion compensation for NBSS-2 will require the modulation of ADC start time and sample-spacing. These will have to be adapted to the TX geometry on a pulse-to-pulse basis. This may also require adding parameter automatic update registers to the ADC strobe circuitry.

Also, as with NBSS-1, the PRF constraints for NBSS-2 will require the development and implementation of an along-track autofocus algorithm.

6.2.2 TX Motion Measurement

The NBSS-2 would presume that the satellite orbit is sufficiently well known to provide nearly adequate TX motion measurement, and TX operation (in a mission sense) is sufficiently well known to provide an indication of where the TX antenna beam is pointed.

System Implications

As before, the effective phase center parameters (and ultimately the effective aperture) will be calculated in the RX. Consequently, coordinate frames for the NBSS-2 likely need to be decoupled from TX and RX vehicles, as well.

For this NBSS-2, traditional autofocus will also be employed, perhaps as a part of the yet-to-be-developed along-track autofocus algorithm, and some degree of clutter-locking is expected to be necessary in this case.

6.2.3 Timing and Synchronization

The NBSS-2 proposes to ascertain the necessary timing information from direct observation of the TX signal.

System Implications

The RX will need to measure the direct TX signal, and remove effects of the TX motion to the best of its ability. It would do this as part of the same pre-aperture signal analysis as that which would derive TX waveform parameters. Subsequent analysis should continue during the phase history data collection, perhaps by a dedicated TX Signal Analysis subsystem.

“I hate to advocate drugs, alcohol, violence, or insanity to anyone,
but they've always worked for me.”
-- Hunter S. Thompson

7 Proposed Bistatic Experiments

The development of a high-performance, fine-resolution, robust and reliable bistatic SAR system is sufficiently complex that an evolutionary strategy is warranted. Towards this end, a series of broad experiments is proposed to integrate and test major subsystems and operational concepts. These are briefly presented below.

Fixed TX, Airborne RX

In this experiment the TX is fixed at a known location, and the RX is airborne. Only a single aircraft is required. This is a common bistatic experiment scenario, with some basic improvements. The purpose here is to demonstrate abilities in the areas of real-time motion compensation, and automatic timing synchronization of the RX to the TX using GPS.

Airborne TX, Fixed RX

In this experiment, the RX is at a fixed location, but the TX is airborne. Only a single aircraft is still required. The purpose here is to force the RX to deal with TX motion. The TX motion and antenna pointing are measured and communicated through a broadcast data channel to the RX.

Airborne TX, Airborne RX

The two prior experiments are combined, using two separate aircraft. This is the first Notional Bistatic SAR System (NBSS-1) previously described. Recall that this requires the RX to have prior knowledge of many aspects of TX operation.

Class 3 Evolution

Subsequent goals would be for the RX to have less and less prior knowledge of TX signal parameters, and less clear knowledge of TX motion. This would be a migration to Class 3 operation. To facilitate cost-savings, many of these experiments could return to an airborne TX with a fixed RX.

Spaceborne TX, Airborne RX

The ultimate goal is to use a spaceborne TX of opportunity, and an airborne RX, consistent with the NBSS-2 previously presented.

“I believe in practicing prudence at least once every two or three years.”
-- Molly Ivins

8 Conclusions

Several points are worth repeating and perhaps relating.

- A high-performance, fine-resolution, reliable bistatic SAR system must be engineered. That is, the separation of the transmitter from the receiver, and the attendant motion differences, requires rethinking a number of issues that are nonproblematic and hence taken for granted in a monostatic SAR.

  For example, the effective phase center for each pulse is neither the transmitter location nor the receiver location, nor the location halfway between them. Furthermore, real-time motion compensation optimally needs to incorporate the instantaneous bistatic angle, as does the calculation of resolution itself.

- For a receiver in a bistatic system, the big issues are

  1) transmitter waveform parameter estimation,
  2) transmitter motion measurement, and
  3) synchronization to the transmitted signal.

- Proper real-time motion compensation can render collected phase history data in such a manner as to considerably aid image formation, just as in the monostatic case. In fact, the bistatic phase history data would differ from its monostatic counterpart to first order by only the inclusion of a nominal bistatic angle term, and perhaps non-optimal azimuth sample spacing.

- In most scenarios of interest, the transmitter has no knowledge of the receiver motion. Consequently, the transmitter is unable to modulate its waveform parameters (including PRF) in an optimal fashion for real-time motion compensation. This leaves real-time motion compensation completely up to the receiver.

- Employing a random phase coding on the transmitted waveform will make undesired bistatic operation by an adversarial receiver difficult, that is, not impossible but much, much harder.

- The bistatic angle is an important parameter to several aspects of bistatic image formation, and consequently the transmitter motion needs to be known to some degree of accuracy.

- Inaccuracy in the transmitter motion data needs to be accommodated by autofocus algorithms, including perhaps an along-track autofocus algorithm. A technique is suggested for accomplishing this.

- GPS appears to be good enough to synchronize the RX and TX to each other. STALO Master Oscillator frequencies could be matched to 1 ppb, and pulse timing should be matchable to within 10 ns.

Figure 6. Two aircraft observing farm scene. (courtesy Miss Taylor Spaulding, 6 ½)

Reference

[1] Nicholas J. Willis (Editor), Hugh D. Griffiths (Editor), *Advances in Bistatic Radar*, ISBN-10: 1891121480, Scitech Publishing, June 30, 2007.

[2] Chad Knight, Mark Jensen, Trevor Jewkes, Jacob Gunther, "FlexSAR multistatic circular SAR collection," *Proceedings of the 2017 IEEE Radar Conference (RadarConf)*, pp. 1542-1546, 2017.

[3] I. Walterscheid, A.R. Brenner, J.H.G. Ender, "Results on bistatic synthetic aperture radar," Electronics letters, Vol. 40, No. 19, pp. 1224-1225, 2004.

[4] Lars MH Ulander, Björn Flood, Per-Olov Frölind, Tommy Jonsson, Anders Gustavsson, Johan Rasmusson, Gunnar Stenström, Arnold Barmettler, and Erich Meier, "Bistatic experiment with ultra-wideband VHF-band synthetic-aperture radar" Proceedings of the 7th European Conference on Synthetic Aperture Radar, pp. 1-4, VDE, 2008.

[5] Jian Li, Petre Stoica, *MIMO radar signal processing*, ISBN-10 : 0470178981, John Wiley & Sons, 2008.

[6] William J. Caputi, Jr., "Stretch: A Time-Transformation Technique," *IEEE Transactions on Aerospace and Electronic Systems*, Vol. AES-7, No. 2, pp 269-278, March 1971.

[7] J. S. Prichard, R. A. Baker, W. J. Capiti, *Analysis for Multistatic Geometric Image Correction*, Rome Air Development Center Report RADC-TR-80-18, Final Technical Report, February 1980.

[8] William J. Caputi Jr., "Image Processing for Bistatic Image Radar," US Patent 4,246,580, January 20, 1981.

[9] William J. Caputi Jr., "Bistatic Imaging Radar Processing for Independent Transmitter and Receiver Flightpaths," US Patent 4.325,065, April 13, 1982.

[10] A. W. Doerry, E. Bishop, J. Miller, V. Horndt, D. Small, "Designing interpolation kernels for SAR data resampling," SPIE 2012 Defense, Security & Sensing Symposium, Radar Sensor Technology XVI, Vol. 8361, Baltimore MD, 23-27 April 2012.

[11] Armin W. Doerry, *Catalog of Window Taper Functions for Sidelobe Control*, Sandia National Laboratories Report SAND2017-4042, Unlimited Release, April 2017.

[12] O. Arikan and D. C. Munson, "A tomographic formulation of bistatic synthetic aperture radar," Proc. ComCon, p. 418, Oct. 1988.

[13] M. Soumekh, "Bistatic synthetic aperture radar inversion with application in dynamic object imaging," *IEEE Trans. Signal Process.*, vol. 39, no. 9, pp. 2044–2055, Sep. 1991.

[14] B. D. Rigling and R. L. Moses, "Polar format algorithm for bistatic SAR," *IEEE Trans. Aerosp. Electron. Syst.*, vol. 40, no. 4, pp. 1147–1159, Oct. 2004.

[15] Can Evren Yarman, Birsen Yazici, Margaret Cheney, "Bistatic synthetic aperture radar imaging for arbitrary flight trajectories," *IEEE Transactions on Image Processing*, Vol. 17, No. 1, pp. 84-93, 2007.

[16] Brian D. Rigling, Randolph L. Moses, "Motion Measurement Errors and Autofocus in Bistatic SAR," *IEEE Transactions on Image Processing*, Vol. 15, No. 4, pp. 1008-1016, April 2006.

[17] Armin W. Doerry, *Radar Receiver Oscillator Phase Noise*, Sandia National Laboratories Report SAND2018-3614, Unlimited Release, April 2018.

[18] G. Yates, A.M. Horne, A.P. Blake, R. Middleton, "Bistatic SAR image formation," IEE Proc.-Radar Sonar Navig., Vol. 153, No. 3, pp. 208-213, June 2006.

[19] Armin W. Doerry, *Reflectors for SAR Performance Testing – second edition*, Sandia National Laboratories Report SAND2014-0882, Unlimited Release, Supersedes SAND2008-0396, February 2014.

[20] Jens Balke, "Field Test Of Bistatic Forward-looking Synthetic Aperture Radar," *Proceedings of the IEEE International Radar Conference*, pp. 424-429, 2005.

[21] Omar J. Jacomini, "Radar system for detecting slowly moving targets," US Patent 4,048,637, September 13, 1977.

[22] J. W. Adams, T. M. Schifani, "Waveform Error Analysis for Bistatic Synthetic Aperture Radar," *Proceedings of the International Radar Conference*, Radar '87, 1987.

[23] John C. Kirk Jr., "Bistatic SAR Motion Compensation," *The Record of the IEEE 1985 International Radar Conference*, Arlington, Virginia, May 6-9, 1985.

[24] Elliott D. Kaplan, *Understanding GPS Principles and Applications*, ISBN 0-89006-793-7, Artech House, Inc., 1996.

[25] Arthur Beiser, *Concepts of Modern Physics – second edition*, ISBN 0-07-004363-9, McGraw-Hill, Inc., 1973.

[26] Charles V. Jakowatz, Daniel E. Wahl, Paul H. Eichel, Dennis C. Ghiglia, Paul A. Thompson, *Spotlight-Mode Synthetic Aperture Radar: A Signal Processing Approach*, ISBN 0-7923-9677-4, Kluwer Academic Publishers, 1996.

[27] Robert F. Ogrodnik, "Bistatic Laptop Radar, An Affordable, Silent Radar Alternative," *The Proceedings of the 1996 IEEE National Radar Conference*, Ann Arbor, Michigan, 13-16 May, 1996.

[28] Gert Retzer, "A Passive Detection System for aWide Class of Illuminator Signals", Conference Record: IEEE ICASSP 79, 1979.

[29] Gert Retzer, "Some Basic Comments on Multistatic Radar Concepts and Techniques," Colloquium Digest: Colloquium on Ground and Airborne Multistatic Radar, Institution of Electrical Engineers (Great Britain), 4 December 1981.

[30] C. K. Bovey, C. P. Horne, "Synchronisation Aspects for Bistatic Radars," *Proceedings of the IEEE International Conference on Radar*, 1987.

[31] Matthias Weiß, "Synchronisation of Bistatic Radar Systems," *Proceedings of the 2004 IEEE International Geoscience and Remote Sensing Symposium*, vol. 3, pp. 1750-1753, 2004.

[32] V. N. Antipov, "The Resolving Power of Semiactive Synthetic-Aperture Radar Systems," Radiotekhnika, No. 5, 1987, English translation from Telecommunications and Radio Engineering, Vol. 41/42, No. 6, June 1987.

[33] Edward D. Powers, Edward C. Jones, Jimmie Brad, *Truetime MK-V 151-301-522 P/Y Code GPS Receiver Live Static Test*, Naval Research Laboratory Report NRL/MR/8150--97-8114, November 24, 1997.

[34] B. L. Burns, J. T. Cordaro, "SAR image formation algorithm that compensates for the spatially variant effects of antenna motion," SPIE Proceedings, Vol 2230, SPIE's International Symposium on Optical Engineering in Aerospace Sensing, Orlando, 4-8 April 1994.

"Now you know the rest of the story."
-- Paul Harvey

Distribution

Unlimited Release

Email—External

Brandeis Marquette	Brandeis.Marquette@ga-asi.com	General Atomics ASI
Jean Valentine	Jean.Valentine@ga-asi.com	General Atomics ASI
John Fanelle	John.Fanelle@ga-asi.com	General Atomics ASI

Email—Internal

all members	534x	
Technical Library	9536	libref@sandia.gov

Sandia National Laboratories is a multimission laboratory managed and operated by National Technology & Engineering Solutions of Sandia LLC, a wholly owned subsidiary of Honeywell International Inc. for the U.S. Department of Energy's National Nuclear Security Administration under contract DE-NA0003525.